Reqs
of Defen
should be

Dep
DDC ser
nizant m

All other persons and organizations should apply to the:

Clearinghouse for Federal Scientific
and Technical Information (CFSTI)
Sills Building
5285 Port Royal Road
Springfield, Virginia 22151

DISCLAIMER NOTICE

THIS DOCUMENT IS THE BEST QUALITY AVAILABLE.

COPY FURNISHED CONTAINED A SIGNIFICANT NUMBER OF PAGES WHICH DO NOT REPRODUCE LEGIBLY.

TECHNICAL OPERATIONS RESEARCH

AFCRL-65-179

RELATIVE ADVANTAGES OF INTERFEROMETER OVER TELESCOPE FOR MEASURING SOURCE SIZES

Helmut Hecksher and George O. Reynolds

Technical Operations Research
Burlington, Massachusetts

Contract No. AF19(628)-3871
Project No. 8663

15 November 1963 to 31 January 1965

FINAL REPORT
5 March 1965
ARPA Order 450, Amendment 2, Task 2

Prepared for

Air Force Cambridge Research Labortories
Office of Aerospace Research
United States Air Force
Bedford, Massachusetts

Burlington, Massachusetts

BLANK PAGE

ABSTRACT

In this report an analysis of the Michelson stellar, Fizeau double-slit and the folding interferometers is given and their relative merits are compared to a telescope for performing source size measurements. The atmospheric effects upon these instruments are examined. Experimental procedures describing the use of the Michelson stellar interferometer are given. Experimental difficulties encountered in the program are also discussed. It is concluded that interferometers are a better instrument than telescopes for source size measurements in the presence of a turbulent atmosphere if information about the source geometry and intensity distribution is available. When the source geometry and intensity distribution are not known, then none of the instruments give an absolute source size measurement under turbulent conditions.

FOREWORD

The work described in this report (TO-B 65-19) was performed by Technical Operations Research for the Electronic Systems Division of the United States Air Force under Contract AF19(628)-3871.

The authors wish to acknowledge the aid of Dr. B. J. Thompson, Dr. G. B. Parrent, Dr. M. J. Beran, Mr. D. A. Servaes, Miss D. Nyyssonen, and Mr. P. F. Kellen who contributed to the research reported.

TABLE OF CONTENTS

TABLE OF CONTENTS (Cont'd.)

LIST OF ILLUSTRATIONS

LIST OF ILLUSTRATIONS (Cont'd.)

LIST OF ILLUSTRATIONS (Cont'd.)

BLANK PAGE

CHAPTER 1

INTRODUCTION

SUMMARY OF OBJECTIVE

PURPOSE

The purpose of this project was to establish the relative advantages of the interferometer over a single aperture instrument, such as a reflecting or refracting telescope, for measuring source diameters in the presence of atmospheric turbulence.

PROBLEMS

Under this contract, Technical Operations Research has studied the relative merits of a stellar interferometer versus a direct imaging system to measure small angular diameters in the presence of a turbulent atmosphere. It was soon clear that the interferometer was far better suited to the task than was the direct imaging system. Further investigation of the interferometric method indicated that it also has limitations. The following facts, however, are well established:

1. A random or turbulent atmosphere produces a deformed wave front incident on the aperture of the measuring instrument.
2. An imaging system requires an undisturbed (unaberrated) wave front in order to provide a sharp image.
3. A spatially random variation in the amplitude and phase of a wave front does not, however, affect the coherence of the wave at the plane of the disturbance.
4. The stellar interferometer determines source size by measuring coherence.

It follows from item 2 above that random phase errors across the aperture of a telescope produce badly aberrated images that make accurate direct measurement impossible. The telescope, in this sense, depends on the integrated effects of the phase errors. On the other hand, the interferometric method requires only the measurement of the modulus of the degree of coherence of the incident wave front.

Therefore, the interferometer need only "see" the field at two different points in the aperture at any given instant. Now, randomly varying the phase relations between the field at the two points affects only the phase of the complex degree of coherence; this results in a shift of the fringes but does not affect the contrast. The following quantitative considerations are presented to illustrate these points.

The minimum diameters of lenses necessary to allow the direct measurement of the diameters of small light sources by means of a telescope with, say, a filar eyepiece are shown in Figure 1 as a function of the angles subtended by the source.* In plotting Figure 1, the condition was imposed that the angular diameter of the source to be measured should be at least twice the diameter of the diffraction disk. To measure the diameter of a source subtending 2×10^{-6} rad would, for instance, require a telescope with an aperture of at least 131 cm! This assumes good astronomical "seeing" conditions. In the presence of any kind of turbulence, a direct measurement of small sources is likely to be difficult no matter how large the lens.

A major advantage of interferometric methods is that, in general, much smaller apertures can be used than those required for direct imaging. The lower limit is set only by the light-gathering requirements of the system, since the diffraction disk evidently has to be of sufficient intensity to be observed visually, measured photoelectrically, or recorded photographically. Previous reports on the subject are somewhat contradictory. Michelson and Pease[1] stated, "The application of interference methods to astronomical measurements is not seriously affected by atmospheric disturbances, and indeed observations by these methods have proved feasible even when the seeing was very poor." Calder,[2] on the other hand, concluded, "The statements frequently found to the effect that, in contrast to what might be expected, the interferometer does not require excellent seeing conditions, are unduly optimistic. Atmospheric conditions appear to be the controlling factor, and seriously restrict the possibilities of interference methods."

If there is any gap between theory and practice, it probably arises from the limitations imposed on the technique by the relatively slow detectors that are

*Instead of the filar eyepiece, the source image could, of course, also be recorded on photographic film and measured after development.

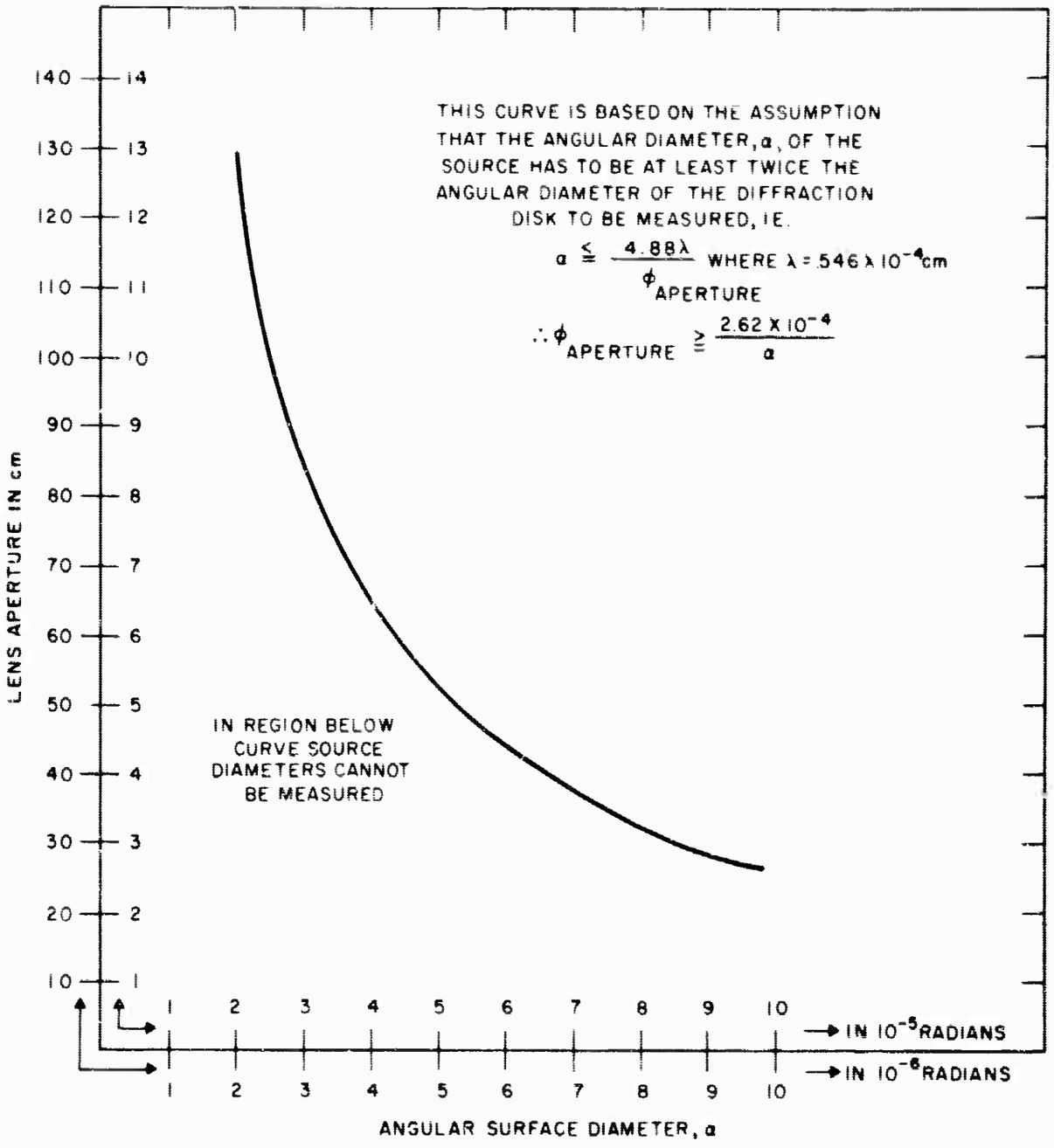

Figure 1. Lens Diameter Necessary to Measure Directly Diameters of Sources as a Function of Angular Source Diameter

presently available. Thus, although the contrast of the fringes is not affected by the atmosphere, the position of the fringes varies randomly in time. If, as is often the case, the frequency of this motion of the fringes is beyond the band pass of the detector, the measured value of the contrast is less than the actual value and the result is that the source diameter as measured is too large. Thus, under typical experimental conditions, photographic detection of fringe contrast would require an integrating exposure of several minutes. This is, of course, prohibitive in all but carefully controlled laboratory experiments. Visually, the situation is often considerably improved. The eye can detect the image in fractions of a second, and typical atmospheric variations are on the order of a few cycles per second. The celebrated experiments of Michelson and Pease used visual detection. Visual detection has also been used in the present Tech/Ops program. However, there are many practical problems where either or both of the following considerations apply:

1. The intensity level is too low for visual detection.
2. Good "seeing" conditions do not exist and one must detect contrast in 10^{-2} to 10^{-3} sec.

The availability of photoelectric detectors of sufficient sensitivity and the development of suitable techniques for photoelectric fringe detection would undoubtedly alleviate some of the difficulties encountered by visual techniques; however, the problem of detecting contrast in these short times has yet to be solved.

Having outlined some of the problems encountered under this program, which seem to indicate that interferometers are more suited to the task of source size measurement in the presence of turbulence, we shall proceed to discuss the various types of interferometers which might be suited for the task.

THE FIZEAU DOUBLE-SLIT INTERFEROMETER

In 1868, Fizeau considered the fringes formed in a Young-type experiment where the two slits were illuminated by light from a double source, namely, two stars close together. A single wavelength was selected and two sets of fringes were produced, one by each source. No interference effects took place between these two sets of fringes, since no coherence existed between the two sources. Hence,

the fringes added in intensity, not in amplitude. If the two sources had similar intensities and the two wavelengths were nearly the same, then two sets of independent interference fringes could be made to superpose exactly and thus sharp fringes be maintained; or the two fringes could be made to almost disappear if displaced by a complete half fringe. The conclusion is that the visibility of the fringes can be varied from 0 to 1 where the visibility of a set of fringes is here defined in the usual way by:

$$\text{Visibility} = \frac{I_{max} - I_{min}}{I_{max} + I_{min}} \qquad (1)$$

By placing a pair of slits of spacing d over the telescope objective, fringes are formed in its focal plane. The intensity of these fringes varies according to a $\cos^2$ law, and their angular separation is λ/d when a single source is viewed. If now another source is also viewed and the two sources have an angular separation of α at the objective, a second set of $\cos^2$ intensity fringes having the same separation is produced. The fringes formed by each source have a different center, and the angular separation of the centers is the angular separation of the sources. If d is now varied until the two sets of fringes have centers separated by half a fringe, then the angular separation of the fringes is known, since the fringe spacing can be accurately determined. Thus, Fizeau was able to measure the angular separation of a double star by varying d until the fringes disappeared; under these circumstances, the angular separation of the double star is $2\lambda/d$. A mathematical analysis of this instrument is given in Chapter 4.

Michelson applied Fizeau's method to the measuring of the diameters of celestial objects. Initially, he measured four of Jupiter's moons using a Lick refracting telescope with slits placed over the objective. Later, acting on a suggestion of Hamy's, Michelson replaced the slit apertures by rectangular apertures, and by using mirrors was able to extend the effective separation of the apertures. More recently, this style of stellar interferometer was used to determine the angular size of celestial radio sources.[3] More recently still, Hanbury-Brown and Twiss[4] made important modifications which are applicable to both radio and visible sources.

THE MICHELSON STELLAR INTERFEROMETER

The construction of the Michelson stellar interferometer is shown in Figure 2. The inner mirrors M_2 and M_3 are fixed, while the outer mirrors M_1 and M_4 are symmetrically movable and perpendicular in axis OA. Light from the distant source after reflection by the mirrors passes through the two apertures S_1 and S_2 and into the telescope objective. Separation of the two beams is given by the separation of the two mirrors M_1 and M_4 and can be made much larger than the aperture of the objective. Therefore, the smallest angular diameter that may be measured is determined by the maximum possible separation of the outer mirrors and not by the diameter of the objective.

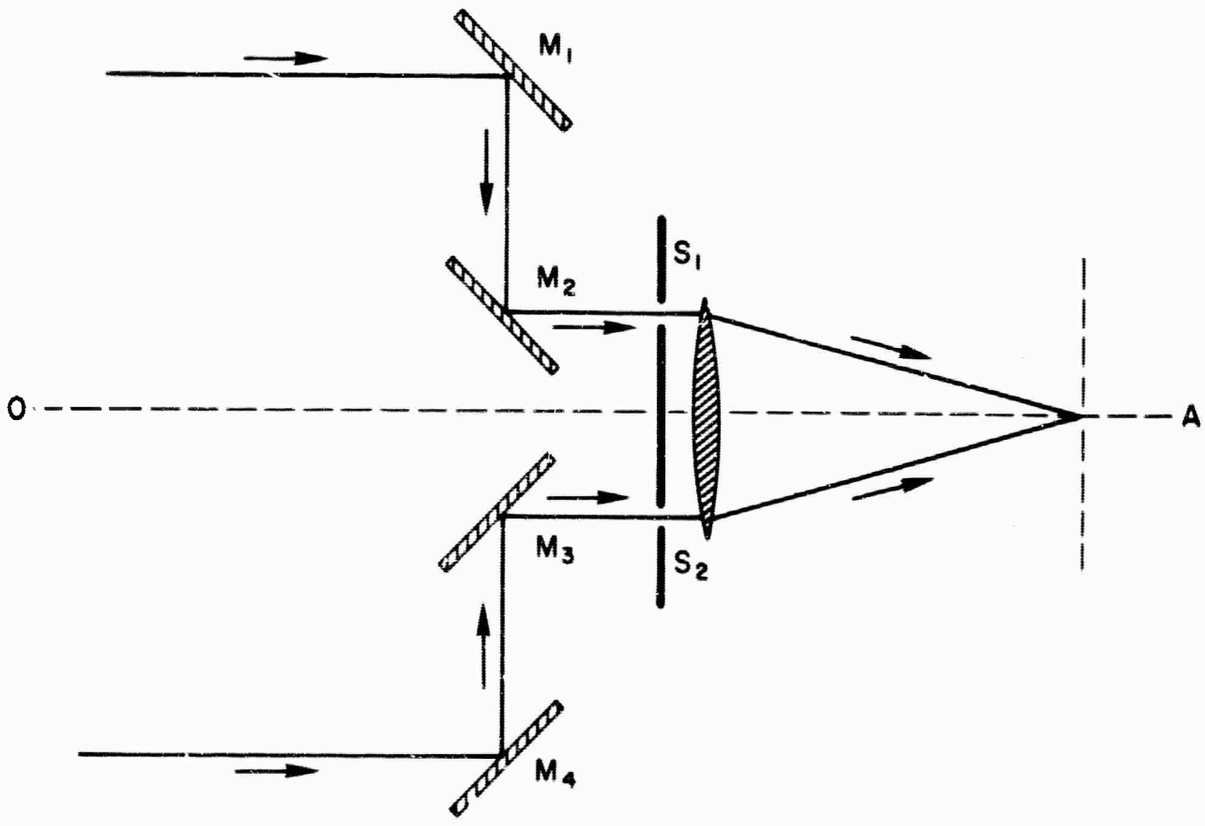

Figure 2. Schematic Diagram of the Michelson Stellar Interferometer

In the image plane of the objective $\cos^2$, intensity fringes are seen. These fringes fall off in intensity on moving out from the axis because of the diffraction envelop of the apertures S_1 and S_2. Consider a system in which S_1 and S_2 are circular apertures. Then by making S_1 and S_2 small, the Airy disc will be large, and a considerable number of fringes will be seen crossing the disc. To determine the source size, mirrors M_1 and M_4 are moved symmetrically until, at some distance d, the fringes vanish. The angular diameter of the star Θ is then given by the expression

$$\Theta = 1.22\,\lambda/d \quad . \tag{2}$$

The method is also adaptable to the measurement of the diameters of microscopic particles that cannot be resolved by the microscope. One important difference between the Michelson and the Fizeau interferometers is that Michelson's is nonstationary (i.e., the fringes and their envelope do not move as a unit in the image plane as the source is moved off-axis). A mathematical description including this effect is given in Chapter 2.

Essentially, the fringes seen in a Michelson interferometer are two-beam interference fringes formed by division of amplitude. If the two beams were completely coherent, then the fringes would have a visibility of 1 and, if incoherent, a visibility of 0. The source to be measured is considered incoherent; but, since light from a single point of the source reaches all points in the field, and therefore each aperture, there is some correlation in the field. By this type of consideration, the visibility of the fringes can be calculated from the known parameters of the system. However, it is more desirable to describe the experiment in terms of modern coherence theory. Indeed, for the Hanbury-Brown and Twiss modification, it is only really understandable from this standpoint.

In coherence theory, the term "partially coherent" is used to describe the interfering beams. The resulting intensity distribution is then given by the following expression

$$I(p) = I_1 + I_2 + 2\sqrt{I_1 I_2}\,|\gamma_{12}|\,\cos\phi_{12} \quad , \tag{3}$$

where I_1 and I_2 are the intensities of the individual beams, and $|\gamma_{12}|$ is the so-called degree of coherence. For the case when $I_1 = I_2$,

$$I(p) = 2I\left(1 + |\gamma_{12}| \cos \phi_{12}\right), \tag{4}$$

and $|\gamma_{12}|$ is equal to the visibility of the fringes.

Experiments to verify Eq. (4) have been carried out and reported in the literature (Thompson and Wolf,[5] Thompson[6]).

FOLDING INTERFEROMETER

The only available description of this instrument, proposed by L. Mertz, appears in a pair of advertisements.[7] This instrument, which Mertz calls a wave-front folding stellar interferometer (Figure 3), is closely related to an earlier model by W. M. Sinton.[8] Since no detailed theoretical treatment of the underlying physics of this interferometer was available, an attempt to mathematically analyze its potential seemed worthwhile. This analysis appears in Chapter 4 and its merits are compared with those of other instruments in Chapter 5.

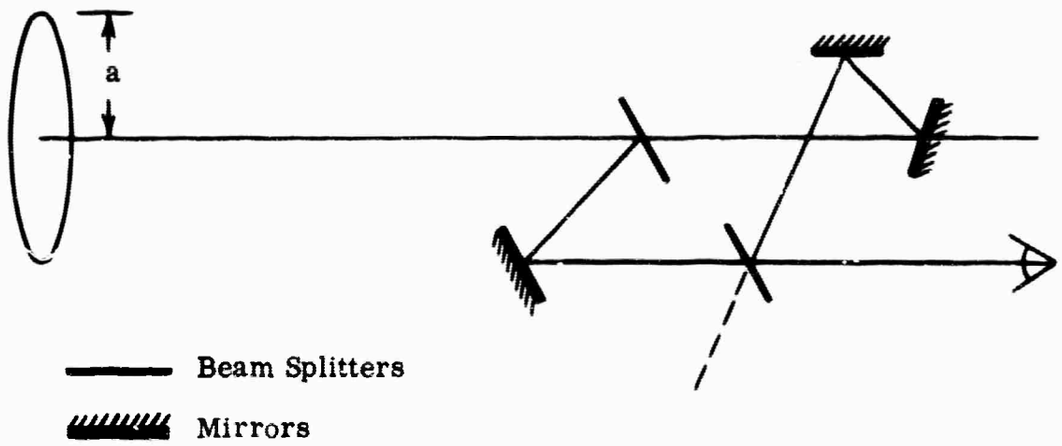

Figure 3. Wave-Front Folding Stellar Interferometer

ATMOSPHERIC EFFECTS

The usual analysis of interferometers (see Chapters 2 and 4) is only applicable to source diameter measurements if the medium between the source and the telescope is completely isotropic and homogeneous. Yet, when using an interferometer to determine the angular size of a star, it is not a good approximation to treat the intervening medium as isotropic and homogeneous. The question then has to be asked: What effect does a real atmosphere have on the fringes in an interferometric experiment?

To answer this question, it is necessary to discuss what anisotropy exists in the atmosphere. To this end, consider a conceptual experiment in which a small optical transmitter is set up in space well above the atmosphere. On the earth, a receiver is set up consisting of a mirror and a detector (photomultiplier). The mirror is directed at the source, and the output power is plotted versus the aperture of the mirror. For quite small mirrors, the power increases as the square of the aperture area. As the aperture is increased still further, however, the received power increases at a slower rate, while for quite large apertures, the received power grows only with aperture size. These are the same effects experienced in scatter communications systems.

The power referred to above is the average power. If the experiment were actually performed, the received power for a given aperture size would be seen to fluctuate about a mean. The fluctuations can be described as Rayleigh noise and have been discussed in detail in the scatter literature.

These results are easy enough to describe. The atmosphere may be considered to be a medium composed of spatially random variations in index of refraction. Furthermore, the atmosphere suffers random rearrangements in time. Thus, a point source located beyond the atmosphere results not in a plane wave incident on the aperture of the receiver, but rather in a highly distorted wave front. The precise shape of this incident wave front depends on the detailed shape of the index variations in the atmosphere at the time of the passage of the wave front. If the scale of the wave-front variation is small compared to the aperture of the receiving antenna (lens or mirror), then the resulting pattern in the focal plane has the appearance in space of Rayleigh distributed noise.

Under these circumstances, the gain of the system will depend on the location of the detector relative to the power distribution in the Rayleigh noise pattern, as illustrated in Figure 4. The light distribution in Figures 4(a) and 4(b) was obtained by allowing a coherent but random wave front to be incident on a collecting aperture. Clearly, if a point detector were used instead of a film, the output of the detector would depend on its location relative to the maxima in this pattern. Since the location of these maxima vary with each rearrangement of the atmosphere, large variations in the output of a point detector are to be expected.

It should be noted that such spatially random patterns do not affect the coherence of the radiation in terms of the Wolf's formalism. Figures 4(a) and 4(b) show the patterns through two different apertures, each of which is large compared to the scale of the wave-front variations. Figure 4(c) shows the interference pattern caused by allowing light from each of these apertures to interfere. It should be noted that at every position in Figure 4(c) where the light is detectable, there are high contrast fringes. Since for quasi-monochromatic illumination the contrast or visibility of interference fringes is identical to the degree of coherence, it must be concluded from Figure 4(c) that the coherence of the radiation was unaffected by passage through the random media. In this experiment, the random noise was introduced by placing ground glass over the two apertures.

To continue the discussion of atmospheric effects, consider next the appearance of the diffraction pattern when the receiving aperture is small compared to the scale of the wave variations. Under these circumstances, the lens sees essentially a plane wave whose direction varies from one instant to the next in a random fashion. The shape of the diffraction pattern is thus the same as it would be if the intervening atmosphere were replaced by free space. The location of this pattern, however, is determined by the random index variations in the atmosphere. These variations are essentially the phenomena responsible for the visually-observed "twinkling of stars." Here the pupil of the eye is certainly small compared to the scale of atmospheric fluctuations. At every instant the eye forms a good image of the star, but this image moves about in a random way on the retina. This random motion of the image is thus interpreted as a "twinkle." While at any instant such a small lens is forming the correct diffraction pattern with the free-space gain, beamwidth, and

(a) The diffraction pattern of an aperture with ground glass placed over it to introduce random noise

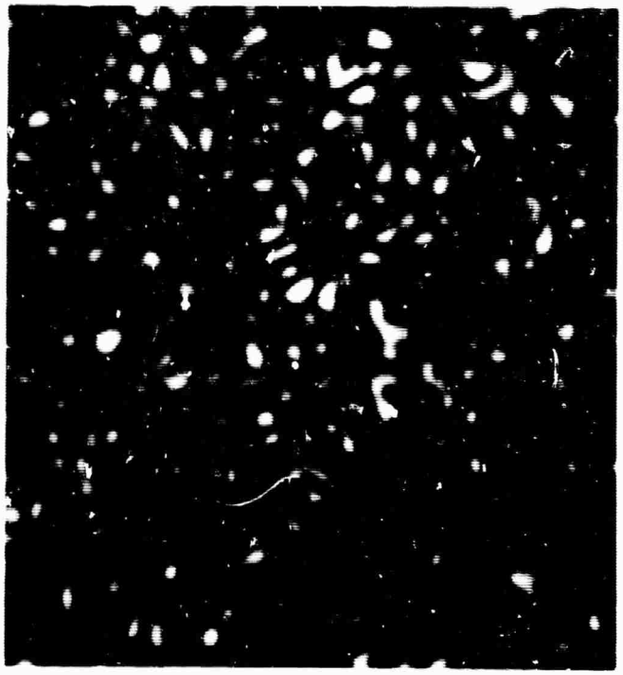

(b) A similar photograph for an identical aperture

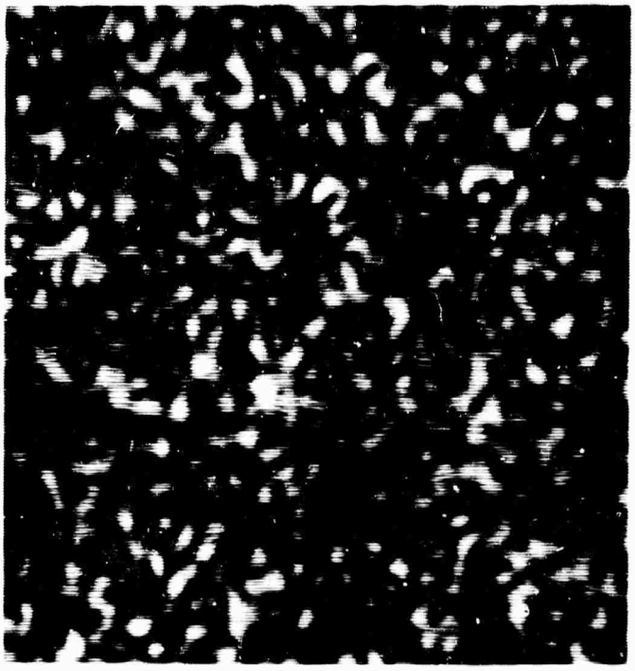

(c) The interference effects introduced by allowing the light from the two apertures to interfere

Figure 4. Effect of Random Noise on the Coherence

side lobe level, it is forming the pattern at the wrong location. In fact, the net gain of such a small receiving aperture will be determined by the location of the detector relative to the location of the maxima of this diffraction pattern. Thus, in this case also, a point detector would observe a random variation in gain.

To provide a single constant description of these phenomena, Beran[9] introduced an ensemble average formalism of coherence theory. In terms of this theoretical picture, the preceding phenomena are described by the following argument. A distinct quasi-monochromatic point source produces a essentially coherent plane wave that impinges on the random media (atmosphere). Although passage through the media does not affect the coherence of the radiation in terms of Wolf's formalism (see Figure 4), it does affect the ensemble averaged coherence. In particular, the finer the scale of the atmosphere variations, the greater is the reduction of the ensemble averaged coherence at a wave front that passes through this medium. The ensemble average diffraction pattern of the receiving aperture may then be described as a diffraction of partially coherent light.

In a series of papers by Parrent and Skinner,[10] Thompson,[11] and Shore,[12] the diffraction of partially coherent radiation has been examined in some detail for a useful class of coherence functions. The results obtained by these authors indicate that the observable characteristics of the diffraction pattern (Strehl definition, beamwidth, side lobe level) depend on the detailed structure of the coherence function, in the diffraction aperture. In fact the characteristics of the diffraction pattern are seen to vary even qualitatively with the form of the mutual coherence function.

In Figure 5, the intensity pattern of a slit illuminated by partially coherent light is plotted in angular coordinates. The curve-to-curve parameter, χ, is the ratio of the aperture size to the coherence interval. In particular, when $\chi = 0$ (when coherent light is incident upon the aperture), the diffraction pattern is a sinc^2 pattern of the diffraction-limited rectangular aperture. As this parameter is varied, the height of the central maximum diminishes, the nulls begin to fill in, and the width of the central maximum and that of the side lobes increases. In Figures 6 and 7 theoretical and experimental curves for a circular aperture illuminated with light having a Besinc correlation (i.e., $2J_1(x)/x$ where $J_1(x)$ is a Bessel function of the first kind) are shown. The agreement between theory and experiment is known to be excellent.

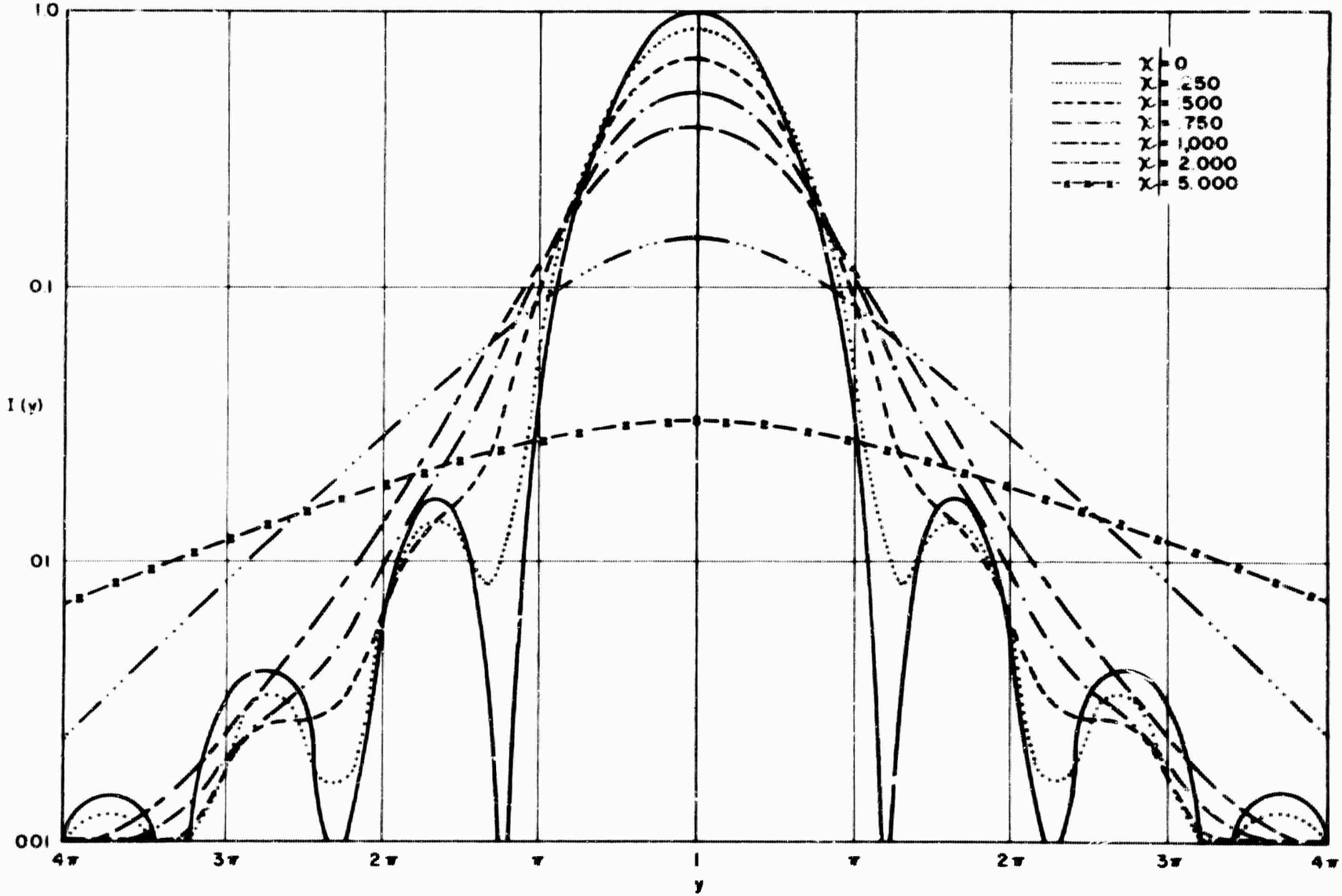

(The parameter χ is the ratio of the aperture size to the coherence interval.)

Figure 5. The Intensity Distribution in the Diffraction Pattern of a Slit Illuminated by Partially Coherent Light

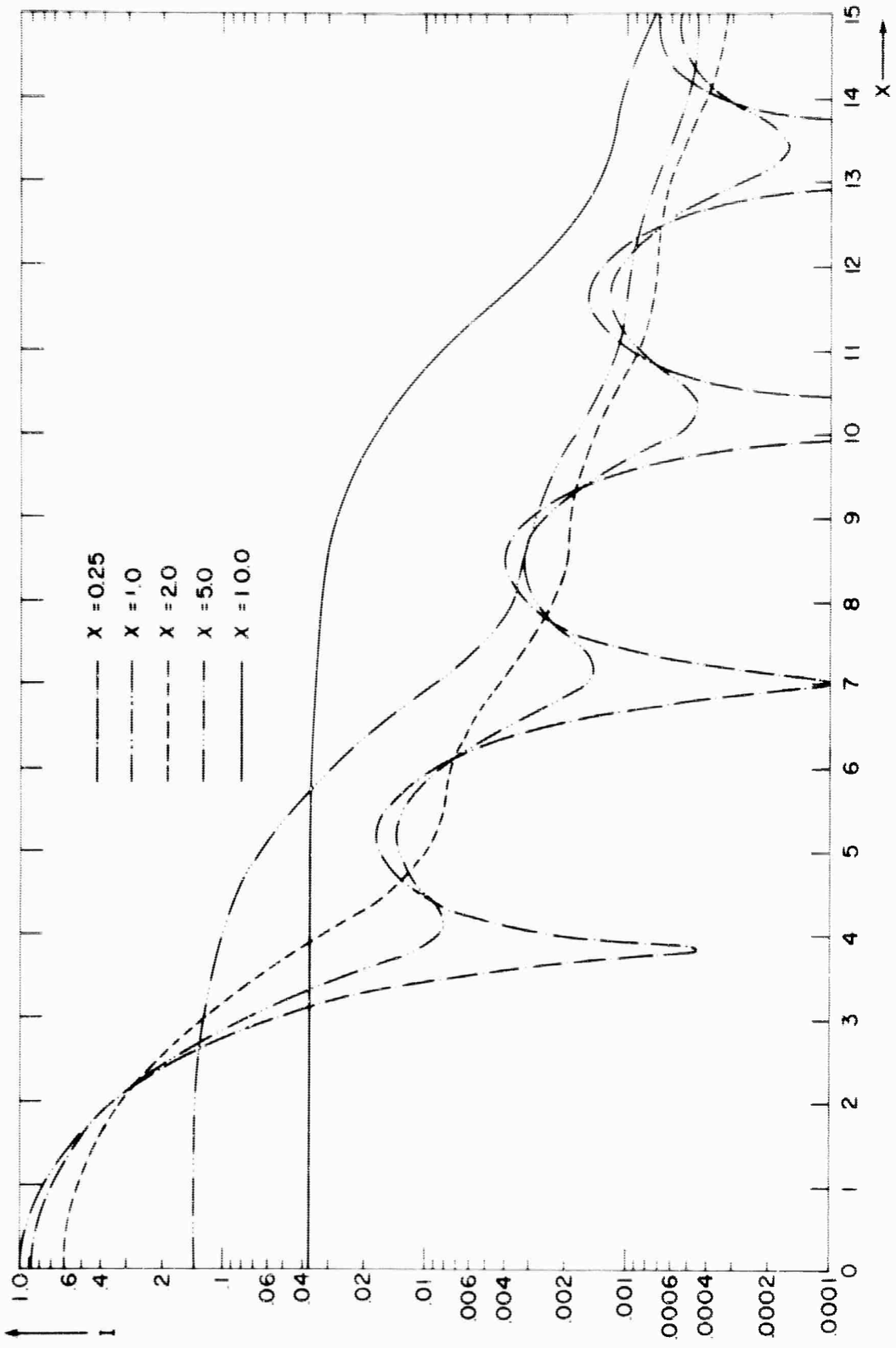

Figure 6. Theoretical Intensity Pattern for a Circular Aperture

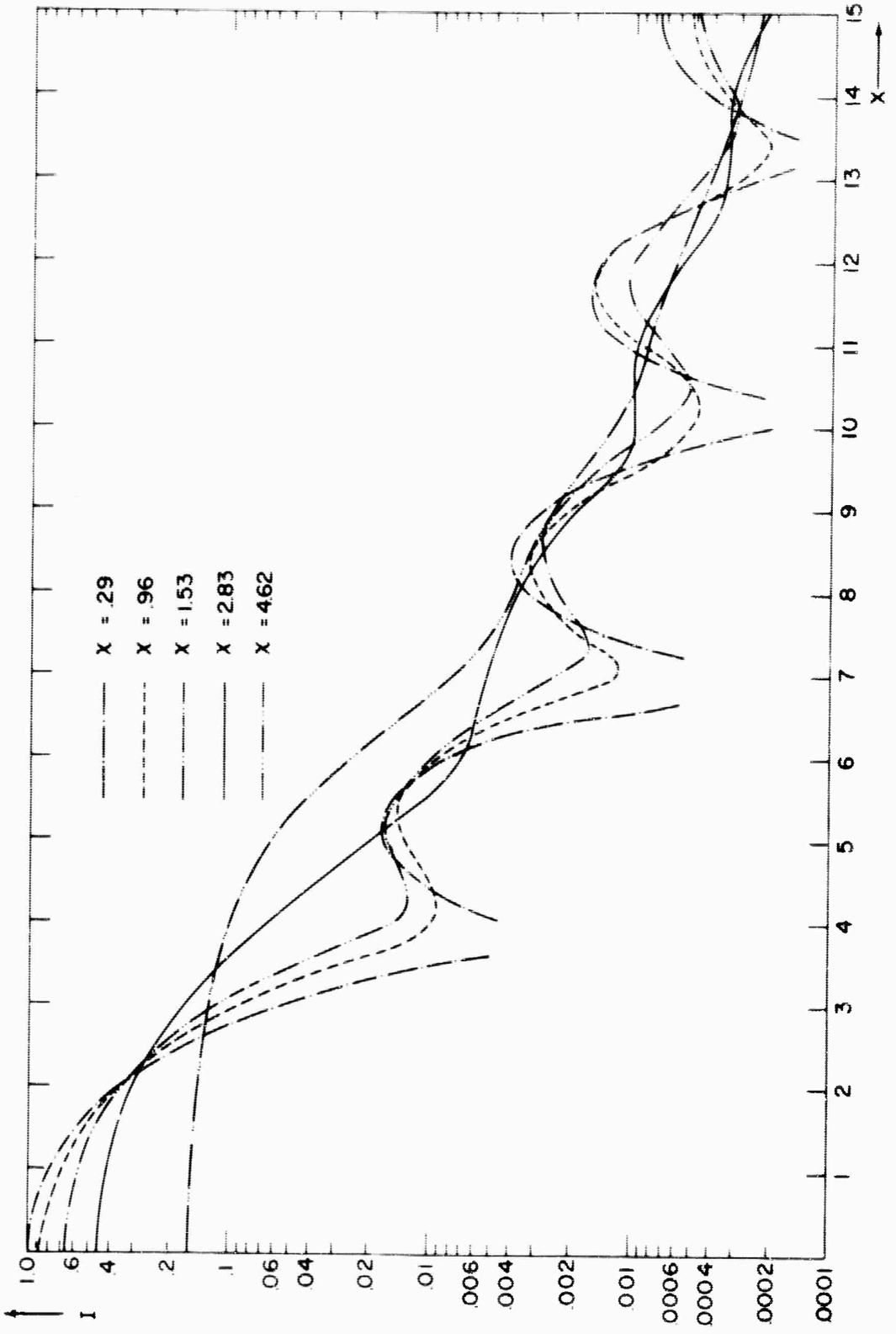

Figure 7. Experimental Intensity Pattern for a Circular Aperture

In the preceding discussion, the atmospheric effects on image quality have been described from two different points of view. From the first point of view, detailed knowledge of the index variations in the atmosphere is required to predict the performance of the given optical system. In the second approach, it is necessary only to know a certain statistical parameter of the atmospheric index variations. In particular, it is important to know that the required parameter, the coherence interval, is determined by the two-point coherence function describing the random media. A complete statistical description of the performance of optical instruments can be obtained by simply measuring the manner in which the index of refraction fluctuates at various points in the atmosphere. Experiments involving essentially point-to-point measurements with a refractometer cannot provide the necessary parameters for the determination of the performance of optical instruments that must look through the atmosphere, except under very special circumstances.

Limitation on the Performance of an Interferometer

In the actual use of a Michelson stellar interferometer, the size of the source, which is incoherent, is measured by setting the spacing of the apertures for zero fringe visibility. In this way, the correlation interval for the light arriving at the instrument is determined. However, the value of the correlation interval is not only determined by the size of the source, but also by the atmosphere. The atmosphere has the effect of making the correlation interval shorter, and, since the correlation interval is a time average, it is the time-averaged atmosphere fluctuations that are important. This means that the answer obtained for the source size is always too large. Therefore, a correction has to be made to allow for the atmospheric effect on the correlation, if an absolute result is being sought.

It must also be realized that the atmosphere sets a limit to the smallest size of source that can be measured by an interferometer. Thus, atmospheric effects, not engineering difficulties, determine the maximum separation of slits. To establish what limits should be set for the separation of these apertures requires a knowledge of the magnitude of the atmospheric effects.

In a laboratory experiment, it is possible to investigate the effect of a simulated atmosphere, because the source size is now a known quantity. Consider the

type of experiment involving two-beam interference by division of amplitude for measurement of the size of an incoherent source set up in the laboratory. If the laboratory atmosphere is considered still, then the source size may be measured. Since a source of known size can be used, the measured diameter may be verified, and hence, if the known and measured diameters agree, then the assumption of a still laboratory atmosphere is valid. The turbulence was introduced quite satisfactorily by using a hot plate and the amount controlled by the voltage applied to the hot plate. When this was done, however, the measurement of the fringe visibility was a difficult problem limiting the usefulness of the instrument.

SUMMARY OF THE WORK DONE

In Chapter 1 we discussed the problem areas encountered in this program and the instruments to be used in measuring source sizes. A general discussion of atmospheric effects upon these instruments was also given. In the remainder of the report (Chapters 2-5) a mathematical description of each instrument will be given as well as a detailed description of the experiments performed during this contract. Some further effects of turbulence upon source size measurements are also discussed. The results compare the relative merits and disadvantages of the particular instruments as source size measuring devices. The analysis given of the folding interferometer and the Fizeau interferometer in Chapter 4 was not performed under this contract. In a subcontract to Block Associates Inc. on the Glow program we were asked to compare the two instruments. Due to their relative importance to the present problem the results are included here for the sake of continuity and completeness.

CHAPTER 2

THEORETICAL CONSIDERATIONS OF THE MICHELSON STELLAR INTERFEROMETER

INTRODUCTION

Some theoretical effort was spent during this contract investigating the stationarity of the Michelson stellar interferometer. T. Holland observed (private communication) that the impulse response of this interferometer was nonstationary. It is of considerable importance to determine what effect this might have on source size measurements; hence, considerable effort was expended to investigate the problem theoretically. (The stationarity of the Fizeau version of the interferometer, which consists of widely spaced double slits and a suitable focusing lens, is not affected by Holland's observation.)

NONSTATIONARITY EFFECTS ON SOURCE SIZE MEASUREMENTS

The careful tracing of rays through the aparatus of Figure 2 shows that no path difference is introduced between the two paths through the interferometer by tipping the wave front through a small angle α to the normal. This result occurs because of the symmetrical design of the original apparatus by Michelson. If the system were stationary, a path difference would be expected between the mirrors and the slits. To show the effect of the nonstationarity on the system, it is advantageous to derive its impulse response, or Green's function. Since the system is linear in intensity, the image intensity can be found by performing the all space integral of the impulse response times the object intensity distribution. The result will then be compared with Michelson's to see what effect the nonstationarity has on the system in measuring source sizes.

The impulse response is defined to be the intensity distribution in the image plane from a distant point source. In Figure 2, represent the apertures as slits of width 2b (see Figure 8), and consider the nature of the disturbance at the slits. If the wave front is tipped through a small angle α to the normal, then the disturbances at corresponding points in the slits in the x plane are out of phase by $(2\alpha)\,2\pi/\lambda$. If half of this phase is associated with each aperture in the x plane, then the

disturbance at the center of the upper slit lags the disturbance at the center of the lower slit; hence, the phase of the disturbance at the upper slit may be written as

$$e^{-ik\alpha x} ,$$

while the phase of the disturbance at the lower slit is

$$ik\alpha(-x) .$$

No additional path difference is introduced in going through the system.

To find the disturbance at a slit in the y plane, a change of variables is made; for $y > o$ (i.e., the upper slit)

$$y = x - (S - s) ,$$

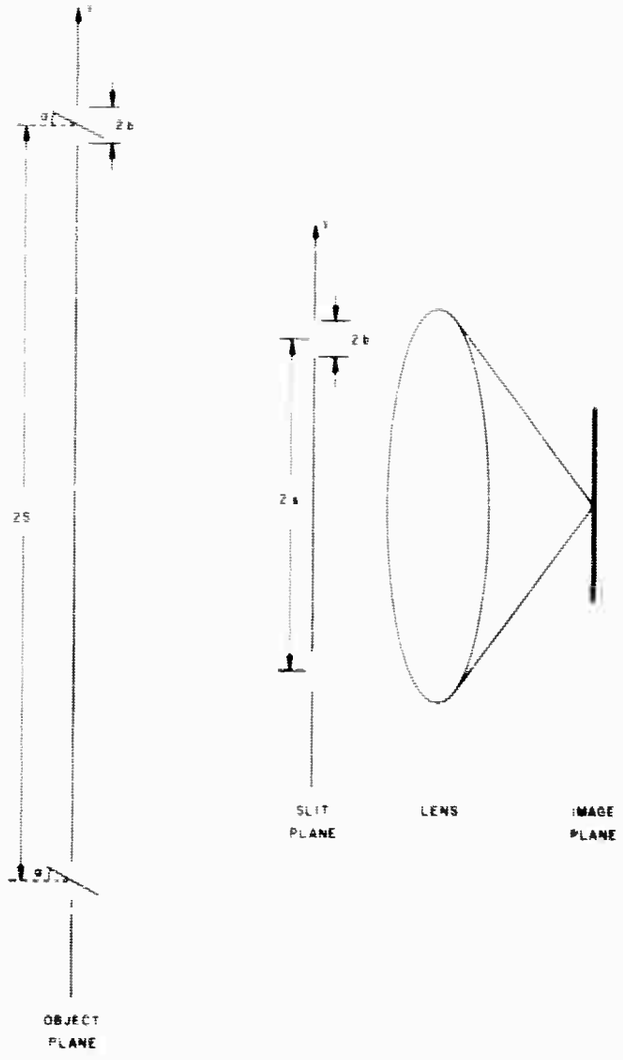

Figure 8. Nomenclature for Stellar Interferometer

where the slit range is $s - b \leq y \leq s + b$; thus the phase at the upper slit in the y plane is

$$e^{-ik\alpha(y + S - s)} . \qquad (5)$$

For $y < o$ (i.e., the lower slit),

$$-x = -y + (S - s)$$

or

$$y = x + (S - s)$$

for the slit range $-s - b \leq y \leq -s + b$ so that the phase at the lower slit in the y plane is

$$e^{-ik\alpha(y-(S-s))} \tag{6}$$

Equations (5) and (6) and their corresponding limits are the aperture distribution for the problem. Using Green's function solution to the wave equation, we find that the image intensity distribution, or the impulse response, is the square of the Fourier transform of this aperture amplitude distribution. The image amplitude is

$$U(\phi, x) = \int_{-s-b}^{-s+b} e^{-ik\alpha(y-(S-s))}\, e^{-iky\phi}\, dy + \int_{s-b}^{s+b} e^{-ik\alpha(y+S-s)}\, e^{-iky\phi}\, dy \tag{7}$$

Let $\alpha + \Theta = \phi$, where α is the angle of tip and Θ is the field angle

$$\begin{aligned} U(\Theta, \alpha) &= \left[\int_{-s-b}^{-s+b} e^{-iky(\alpha+\Theta)}\, dy\right] e^{+ik\alpha(S-s)} \\ &\quad + \left[\int_{s-b}^{s+b} e^{-iky(\alpha+\Theta)}\, dy\right] e^{-ik\alpha(S-s)} \\ &= e^{ik\alpha(S-s)} \int_{-s-b}^{-s+b} e^{-iky\phi}\, dy + e^{-ik\alpha(S-s)} \int_{s-b}^{s+b} e^{-iky\phi}\, dy \end{aligned} \tag{8}$$

Making the change of variables

$$y = y' - s \text{ in the first integral}$$

and

$$y = y' + s \text{ in the second integral} ,$$

we obtain

$$U(\Theta, \alpha) = \left[e^{ik\left[\alpha(S-s) + s\phi\right]} + e^{-ik\left[\alpha(S-s) + s\phi\right]} \right] \int_{-b}^{b} e^{-iky'\phi}\, dy' .$$

Performing the integral, rewriting the exponential term, and squaring the answer yields

$$g(\Theta, \alpha) = |U(\Theta, \alpha)|^2 = 16\, b^2\, \mathrm{sinc}^2 \frac{2\pi b\phi}{\lambda} \cos^2 \frac{2\pi}{\lambda}(\phi s + (S-s)\alpha) \qquad (9)$$

In Eq. (9), $g(\Theta, \alpha) \neq g(\Theta + \alpha)$ alone, so convolution type integrals involving this impulse response are not possible. This characteristic is called the nonstationarity of the system. (Note: if S = s the system is stationary. This case is just the Fizeau interferometer.)

What additional effect does this additional phase in the cosine term have on the system? To answer this question we must actually image a source through this linear system and perform the resulting integral.

If the source distribution is represented by $I_o(\alpha)$ over the physical source, then

$$I_{im}(\Theta) = \int_{-\alpha_o}^{\alpha_o} I_o(\alpha)\, g(\Theta, \alpha)\, d\alpha , \qquad (10)$$

where $g(\Theta, \alpha)$ is the impulse response given by Eq. (9). Substituting Eq. (9) into Eq. (10) and expanding the $\cos^2$ term yields

$$\frac{2I_{im}(\Theta)}{16\,b^2} = \int_{-\alpha_o}^{\alpha_o} I_o(\alpha)\,\mathrm{sinc}^2\,\frac{2\pi b}{\lambda}(\Theta+\alpha)\left[1+\cos 4\pi\frac{(\Theta+\alpha)s}{\lambda}\cos 4\pi\frac{(S-s)\alpha}{\lambda}\right. \tag{11}$$

$$\left. -\sin 4\pi\frac{(\Theta+\alpha)s}{\lambda}\sin 4\pi\frac{(S-s)\alpha}{\lambda}\right]d\alpha = I_1 + I_2 - I_3 \ .$$

Fourier-transforming such relationships yields

$$\frac{\tilde{I}(\mu)}{8\,b^2} = \sum_i \tilde{D}_i(-\mu)\,\tilde{f}_i(\mu) \ . \tag{12}$$

Using Eqs. (11) and (12), we obtain

$$\tilde{I}_1(\mu) = \int_{-\infty}^{\infty}\int_{\alpha_o}^{\alpha_o} I_o(\alpha)\,\mathrm{sinc}^2\,2\pi b(\Theta+\alpha)\,d\alpha\,e^{-2\pi i\mu\Theta}\,d\Theta \ .$$

Representing the spatial star distribution by $D(\alpha)$ for all space and using Eq. (12), we find that

$$\tilde{I}_1(\mu) = \tilde{D}i-\mu)\,\tilde{i}(\mu) \ ;$$

let

$$D(\alpha) = 1 \qquad -\alpha_o \le \alpha \le \alpha_o$$

$$0 \qquad -\alpha_o > \alpha > \alpha_o$$

$$S(x) = \mathrm{sinc}\,(2\pi x) \tag{13}$$

$$T(b/\mu) = \left\{ \begin{array}{ll} 2b - |\mu| = \text{a triangular function} & |\mu| \leq 2b \\ 0 & |\mu| > 2b \end{array} \right\}$$

$$b' = \frac{b}{\lambda} ,$$

$$\frac{S - s}{\lambda} = \Delta' ,$$

$$\frac{s}{\lambda} = s' .$$

Using this notation, we see that

$$\tilde{I}_1(\mu) = 2\alpha_o \, S(\alpha_o \mu) \frac{1}{4b'^2} \, T(b'/\mu) . \qquad (14)$$

Similarly, we obtain

$$\tilde{I}_2(\mu) = \tilde{D}_2(-\mu) \, f_2(\mu)$$

where

$$\tilde{D}_2(-\mu) = \int_{-\infty}^{\infty} e^{-2\pi i(-\mu)} \, D(\alpha) \cos 4\pi\Delta' \alpha \, d\alpha$$

$$f_2(\mu) = \int_{-\infty}^{\infty} \text{sinc}^2 \, 2\pi b' \phi \cos 4\pi s' \phi \, e^{-2\pi i \mu \phi} \, d\phi ,$$

where $D(\alpha)$ is given by Eq. (13). Since the Fourier transform of the cosine is two δ functions, these integrals become

$$\tilde{D}_2(-\mu) = \alpha_o \left\{ S\left[\alpha_o(\mu - 2\Delta')\right] + S\left[\alpha_o(\mu + 2\Delta')\right] \right\}$$

and

$$\tilde{f}_2(\mu) = \frac{1}{4b'^2} \frac{1}{2} \left\{ T(b'/\mu - 2s') + T(b'/\mu + 2s') \right\} ,$$

so that

$$\tilde{I}_2(\mu) = \frac{\alpha_o}{8b'^2} \left\{ S\left(\alpha_o(\mu - 2\Delta')\right) + S\left(\alpha_o(\mu + 2\Delta')\right) \right\}$$

$$\times \left\{ T(b'/\mu - 2s') + T(b'/\mu + 2s') \right\} . \qquad (15)$$

Similarly, we find that

$$\tilde{I}_3(\mu) = \tilde{D}_3(-\mu)\, \tilde{f}_3(\mu) ,$$

where

$$D_3(-\mu) = \frac{1}{2i} \int_{-\infty}^{\infty} e^{-2\pi i(-\mu)\alpha} \int_{-\infty}^{\infty} D(\xi)\, e^{2\pi i \alpha \xi} \left(e^{2\pi i 2\Delta' \alpha} - e^{-2\pi i 2\Delta' \alpha} \right) d\alpha\, d\xi$$

$$= \frac{1}{2i} \int_{-\infty}^{\infty} \tilde{D}(\xi) \left[\int_{-\infty}^{\infty} e^{2\pi i \alpha(\mu + \xi + 2\Delta')} - e^{2\pi i \alpha(\mu + \xi - 2\Delta')}\, d\alpha \right] d\xi ;$$

D is given by Eq. (13) and S is a symmetric function so

$$\tilde{D}_3(-\mu) = \frac{\alpha_o}{i}\left[S\left(\alpha_o(\mu + 2\Delta')\right) - S\left(\alpha_o(\mu - 2\Delta')\right)\right] \tag{16}$$

and

$$\tilde{f}_3(\mu) = \frac{1}{8b'^2 i}\left\{T(b'/\mu - 2s') - T(b'/\mu + 2s')\right\} \quad . \tag{17}$$

Combining Eqs. (16) and (17) yields

$$\tilde{I}_3(\mu) = -\frac{\alpha_o}{8b'^2}\left[S\left(\alpha_o(\mu + 2\Delta')\right) - S\left(\alpha_o(\mu - 2\Delta')\right)\right]$$

$$\times \left\{T(b'/\mu - s') - T(b'/\mu + 2s')\right\} \quad . \tag{18}$$

Substituting Eqs. (14), (15), and (18) into Eq. (12), we see that

$$\tilde{I}(\mu) = 2\alpha_o\lambda^2\left[2T(b'/\mu)\, S\left(\alpha_o\mu\right) + S\left(\alpha_o(\mu - 2\Delta')\right) T(b'/\mu + 2s')\right.$$

$$\left. + S\left(\alpha_o(\mu + 2\Delta')\right) T(b'/\mu - 2s')\right] \quad . \tag{19}$$

To find the image intensity distribution in the image plane, we must take the inverse Fourier transform of Eq. (19). This leads to a cumbersome answer which will not be included since it gave no more information than the special cases which we shall now consider.

CASE I

Assume that T is so narrow compared to S that it is essentially a δ function centered at its μ argument. Physically, this corresponds to the case of point

collectors or infinitesimally small slits in the interferometer. Taking the inverse Fourier transform of Eq. (19) and using the symmetric property of S yields

$$I_{im}(\Theta) = 2\alpha_o\lambda^2 \left\{ 2S(o) + 2S\left(\alpha_o 2(s' + \Delta')\right) \right\} 2 \cos 4\pi s' \Theta \qquad (20)$$

where S(o) = 1. The contrast of the fringes, or the coherence given by

$$g_{12} = \frac{I_{max} - I_{min}}{I_{max} + I_{min}} \quad , \qquad (21)$$

is

$$S\left(\frac{2\alpha_o S}{\lambda}\right) \quad . \qquad (22)$$

This function is zero when the argument of S equals π. The source size is given by

$$2\alpha_o = \frac{\lambda}{2S} \quad . \qquad (23)$$

This is the same result obtained by Michelson. For circular apertures

$$2\alpha_o = \frac{1.22\lambda}{2S} \quad . \qquad (23a)$$

CASE II

Assume that the sinc functions in Eq. (19) are constant. Physically, this means that the source is a point represented by a δ function that is always completely unresolved. Fourier-inverting Eq. (19) under such conditions yields

$$I(\Theta) \propto 2 \left[\int_{-\infty}^{\infty} T(b'/\mu)\, e^{2\pi i \mu \Theta}\, d\mu \right] (1 + \cos 4\pi s' \Theta) \quad , \qquad (24)$$

showing that the contrast of the fringes is unity.

CASE III

Assume that the slit size is finite. Obviously, the star must be so small that it cannot be resolved by the aperture 2b. If this aperture could resolve the star, the outer mirrors would not be necessary in the apparatus because the source size would be directly obtainable in the absence of turbulence.

The resolution of the aperture is

$$R = \frac{\lambda}{2b} \ ;$$

since the star is unresolvable by the aperture,

$$\alpha_o << \frac{\lambda}{4b} \ . \tag{25}$$

Therefore, in Eq. (19) the sinc functions are very broad compared to the triangular functions and may be treated as constant over the range of the triangular function. With this assumption, a Fourier inversion of Eq. (19) shows

$$I_{im}(\Theta) = 4\alpha_o\lambda^2 \cdot \left[\int_{-\infty}^{\infty} T(b'/\mu)\, e^{2\pi i \mu \Theta}\, d\mu\right] \left[1 + S\left(2\alpha_o(s' + \Delta')\right) \cos 4\pi s' \Theta\right] , \tag{26}$$

and the contrast of the fringes is

$$S\left(\frac{2\alpha_o S}{\lambda}\right) ,$$

which yields Michelson's result.

CONCLUSION

Case III covers most cases of physical interest for which the stellar interferometer would be used. Cases for which the sinc function cannot be treated as constant would be those where

$$\alpha_o \sim \frac{\lambda}{4a}$$

(i.e., the star is resolvable by the telescope aperture). In this event, the Michelson stellar interferometer is not necessary because either the Fizeau interferometer or the telescope will enable a source size measurement to be made.

It may be concluded that, even though the stellar interferometer of Michelson is nonstationary (i.e., the fringes and envelope do not move as a unit in the image plane when the source is moved off axis), the source size is still given by Michelson's classical result that the coherence function is

$$S\left(\frac{2\alpha_o S}{\lambda}\right)$$

and the resulting source size is

$$2\alpha_o = \frac{\lambda}{2S} \quad .$$

The nonstationarity of the system does not matter as long as condition (Eq. (25)) is obeyed. This apparently covers all cases of practical interest.

EFFECTS OF TURBULENCE ON ANGULAR DIAMETER MEASUREMENTS USING AN INTERFEROMETER

In this section we shall outline the method for measuring the angular diameter between two distant, incoherent, quasi-monochromatic point sources using interference experiments. We shall use arguments similar to those first given by Michelson. The nonturbulent case will be considered initially and then the turbulent.

When two point sources S_1 and S_2 are very distant, the radiation impinging upon the measuring apparatus may be represented by two plane waves. Referring to Figure 9, we consider the plane wave originating at S_1 to propagate perpendicularly to screen A and the plane wave from S_2 to propagate at angle Θ to the wave from S_1. P_1 and P_2 are two pinholes on screen A a distance d apart. The screen B is taken to be in the far field of the two pinholes in A.

The fringe intensity pattern due to the source S_1 above is shown by the solid line on B. The maximum intensity is at M_1 and the minimum at N_1. The minimum

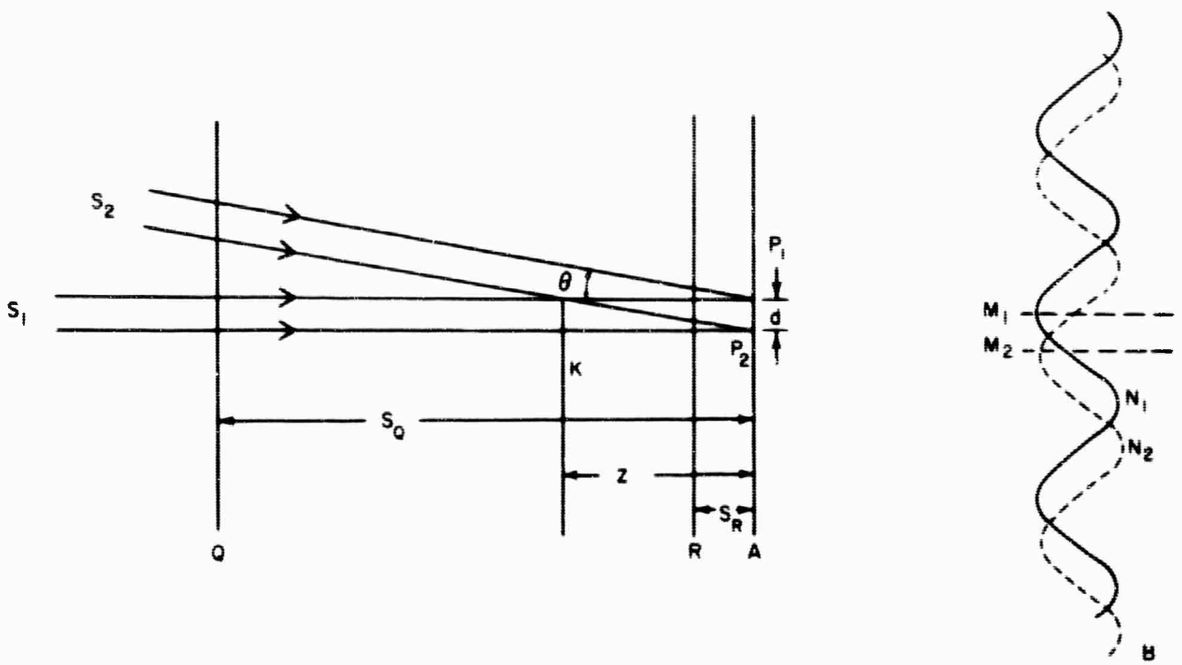

Figure 9. Spatial Relationship Between Two Sources and Interferometer

point occurs because the rays from P_1 and P_2 are out of phase here. The fringe intensity pattern resulting from S_2 above is given by the dotted line. Since the two sources are taken to be incoherent, the intensities on the screen add, and the observed fringe pattern is the sum of the individual patterns.

If d is very small, M_1 and M_2 will almost coincide and the sum of the two individual patterns will exhibit very sharp fringes. As d increases, however, M_1 and M_2 separate, and eventually M_2 coincides with N_1. At this point the sum pattern exhibits no fringes (assuming S_1 and S_2 are of equal intensity). For fixed Θ the distance d for which M_2 and N_1 coincide, say d_M, determines Θ. Calculation shows that $\Theta = \bar{\lambda}/2d_M$ ($\bar{\lambda}$ is the mean radiation wavelength).

Thus, in the absence of turbulence, one need only observe the fringes on B as a function of d to determine the angular diameter of two distant, incoherent, quasi-monochromatic point sources. Note that we must use quasi-monochromatic light since the fringe wavelength (distance between M_1 and the next peak) depends upon

the radiation wavelength. Further, all path-length differences we consider must be less than $c/\Delta\nu$ ($\Delta\nu$ is the frequency spread of the radiation, c is the velocity of light).

When turbulence is present, the picture given above may or may not basically change. We will consider here only turbulent fields in which the characteristic period of turbulent change, τ_t, is very long compared to $1/\Delta\nu$. In times short compared to τ_t but long compared to $1/\Delta\nu$, the radiation thus passes through a medium that may be considered fixed in time. In this medium, however, the index of refraction varies with position in contrast to the nonturbulent case.

In times short compared to τ_t, the radiation from S_1 alone is scattered prior to reaching P_1 and P_2. If, however, the additional path lengths introduced are still $<< c/\Delta\nu$, then the pattern displayed on B will still be a cosine pattern for averaging times short compared to τ_t. If one observed the fringe pattern on B as a function of time, one would see the fringes move about as t exceeded τ_t, but remain stationary for times much less than τ_t. If we are able to observe both S_1 and S_2 separately, we should observe two cosine patterns moving about as a function of time.

If the two cosine patterns do not move relative to each other and thus the distance from M_1 to M_2 remains fixed for fixed d, then we can determine the angular diameter of the source by measuring the fringe visibility for times short compared to τ_t. In this case, the turbulence does not disturb our measurement of angular diameter, it only forces us to make our measurements in times short compared to τ_t.

If the two cosine patterns do move relative to each other, then we cannot determine the angular diameter of the source. In this case a separation d may yield no fringes at time t, and significant fringes at time t_2 if $t_2 - t >> \tau_t$. The utility of interferometric measurements to determine angular source size thus requires that the cosine pattern resulting from S_2 not move relative to the cosine pattern from S_1 for times much greater than τ_t.

To determine if the cosine patterns move in phase, we return to Figure 9. Consider two cases: (a) the atmosphere extends from A to Q; (b) the atmosphere

extends from A to R. In case (a) the rays from S_2 do not cross the rays from S_1 until well beyond the plane Q for the value of d shown. If this is the case when $d = d_M$, then the radiation from S_2 may experience for the most part a different turbulent field than the radiation from S_1. It will experience a different field if a turbulent scale is of the order of d or less. Here we should expect to find that the fringes shift relative to each other for large t.

When all the turbulent eddies important for scattering have a scale much greater than d, the situation is more favorable. In this case the radiations from S_1 and S_2 experience the same turbulent field and we should again expect the cosine patterns to move in phase.

In case (b) the radiation reaching P_1 (or P_2) from S_1 and S_2 experiences almost the same turbulent field, and we expect the fringes to move together. In this case we would hope to be able to measure the angular diameter Θ even in the presence of a turbulent field.

The crossover point K depends upon both Θ and d_M. As we mentioned above, $d_M = \bar{\lambda}/2\Theta$ and thus the distance z may be determined. We find $z = \bar{\lambda}/2\Theta^2$ for $\Theta \ll 1$. The criteria for determining the critical Θ is thus $z/S = \bar{\lambda}/2S\Theta^2 = 1$.

Assuming a sensible atmosphere of about 10 km and a wavelength of light of 5×10^{-5} cm, we have the relation

$$\frac{z}{S} = \frac{2.5 \times 10^{-11}}{\Theta^2}$$

so that $z/S = 1$ at roughly $\Theta = 10^{-5}$ rad. We note that 10^{-5} rad $\approx$ 2 sec.

The same arguments as given above apply to a continuous source distribution of diameter D. Here, however, the constants change somewhat since we must add up a large number of cosine patterns, not just two patterns. The rough figure 10^{-5} is still a good order-of-magnitude number.

The angular diameter of the star 2 Orionis first measured in this manner by Michelson and Pease was 0.055 sec, so that good measurements could be made in spite of atmospheric turbulence. If one chooses to measure the angular diameter

of a 10-m object at 100 km, however, $\Theta = 10^3/10^7 = 10^{-4}$ and the method would be expected to fail if the turbulent scale is of the order of $d_M \approx 0.5$ cm. In the atmosphere, the microscale of turbulence is of the order of millimeters.

It is interesting to note that these arguments explain why planets do not twinkle as much as stars. The angular diameter of Saturn is ≈ 20 sec and the angular diameter of Jupiter is ≈ 50 sec. Using the formula

$$\frac{z}{S} = \frac{d}{\Theta S}$$

where now we take d as the size of the pupil (say 0.5 cm), we have

$$\frac{z}{S} = \frac{0.5 \times 10^{-6}}{\Theta}$$

or $\Theta \approx 10^{-6}$.

Stars have angular diameters less than 10^{-6}. Hence, the rays from all directions experience the same turbulent field and the fluctuation in intensity may be large. For planets, $\Theta > 10^{-6}$ and the rays from different directions experience different turbulent fields, and the intensity fluctuations tend to cancel somewhat.

SUMMARY

In this chapter we discussed theoretically the Michelson Stellar Interferometer and some effects of turbulence on source size measurements. It was seen that the nonstationarity of the Michelson stellar interferometer has no effect upon source size measurements made by the instrument. The Fizeau and Mertz interferometers, which are also used for source size measurements were recently studied at Tech/Ops in a subcontract to Block Associates, Inc. for the Glow Program. The results of this study are included in Chapter 4. In Chapter 5 the instruments are compared. In the next chapter the experimental program performed under this contract is discussed.

CHAPTER 3

EXPERIMENTAL STUDIES

FIZEAU DOUBLE-SLIT INTERFEROMETER

PRELIMINARY EXPERIMENTS

Preliminary experiments were made to ascertain some of the critical parameters for future work. A Fizeau double-slit interferometer was used. The source consisted essentially of a pinhole illuminated by a high pressure mercury arc through a 5461 Å interference filter. A 66-cm focal length lens was mounted 300 cm from the pinhole, its focal plane about 85 cm from the lens. One of a set of diffracting apertures, each with two holes 0.074 cm in diameter, was positioned close to the lens. The holes were 0.5, 1.0, 1.8, 2.0, and 2.2 cm apart. The two small apertures were placed in front of the much larger telescope aperture. As the small circular apertures initially adjacent were moved apart, the visibility, g_{12}, of the two-beam intereference fringes in the focal plane of the telescope decreased until at a distance

$$2S_{ext} = \frac{1.22\lambda}{2\alpha_o}$$

the visibility had become zero (see Eq. (23a)).

This was checked experimentally with a 100-μ diameter pinhole. With the diffraction apertures as far as 1.8 cm apart, interference fringes were visible in the focal plane. At 2.0 cm, they disappeared; at 2.2 cm, they reappeared. This is in accord with the coherence function. Taking $2S_{ext}$ = 2.0 cm, we obtain

$$2\alpha_o = \frac{1.22 \times 0.546 \times 10^{-4}}{2} = 0.0334 \text{ mrad} .$$

This corresponds to a pinhole diameter of $0.0334 \times 10^{-3} \times 300$ cm = 0.01 cm = 100 μ in agreement with the actual diameter used.

A heated wire was then placed at various distances between the pinhole and the diffracting apertures. The visibility of the fringes as judged by the eye seemed

relatively unaffected by the resulting air convection currents. Occasionally, however, a slight blurring took place that seemed to coincide with a rapid movement of the image disc.

A direct measurement of the source diameter was attempted by removing the diffracting apertures and observing the aerial image with a microscope equipped with a filar eyepiece. The demagnified image of the pinhole is $100\,\mu \frac{85\text{ cm}}{300\text{ cm}} = 28\,\mu$ in diameter. The radius of the lens diffraction pattern, $r = 1.22\,f\lambda/\text{Lens aperture} = 7.2\,\mu$ for the arrangement described. Although the image is resolved, its apparent diameter is therefore increased by about $14\,\mu$. An accurate measurement would necessitate an intensity scan along the diameter and a measurement of the distance between two points at which the intensity is one half of its maximum value. The image disintegrated when a heated wire was introduced in the region between the pinhole and the lens.

An evaluation of a photographic interferometric technique to measure the diameter of sources was also begun. Under certain conditions (which were met in these experiments) the coherence factor can be shown to be equal to the visibility factor,

$$g_{12} = \frac{I_{max} - I_{min}}{I_{max} + I_{min}}$$

(see Eq. (21)); and since for circular apertures

$$g_{12} = \frac{2J_1(x)}{x}$$

where $J_1(x)$ is the Bessel function of the first kind, a knowledge of any value (not necessarily zero) of g_{12} for a given value of d should make it possible to determine the scale of the abscissa and hence of $2S_{ext}$.

To test this method, source diameters of 25 and $100\,\mu$ were used. The resulting fringe patterns formed by the Fizeau type interferometer were recorded on Pan X film. The film was developed in D-76 for 15 min to a gamma of unity, and was then scanned by a Joyce-Loebl microdensitometer. Using a D log E curve,

we translated the D_{max} and D_{min} values into I_{max} and I_{min} and hence into g_{12} for a given value of 2S. The resulting values for the diameter of the pinhole were too high; i.e., the experimental values for g_{12} were too low. One or more of the following factors may be responsible for the loss in contrast:

1. Film Characteristics -- The modulation transfer function of the film depends both on intrinsic factors, such as grain size, grain distribution, and film thickness, and on extrinsic factors, such as exposure, type of developer, method of agitation, and the like. For fringe spacing of 10 lines/mm or more, some reduction in film response must be expected. Quantitative data for the film response under the stated conditions have not as yet been obtained.
2. Film was not quite in the focal plane of the lens.
3. Vibrations in the building were transmitted to the components on the optical bench.
4. Aberrations were present in the lens.
5. Errors were introduced by the microdensitometer.

FURTHER EXPERIMENTS

In the preceding sections, a Fizeau interferometer has been briefly described and some measurements of source diameter were reported. These and subsequent measurements using fringe extinction as a criterion were relatively unaffected by air turbulence and agreed to within about 10% with the actual source diameter used. A direct measurement of the image, on the other hand, under the same conditions of turbulence was difficult, if not impossible. This difficulty is illustrated in Figure 10. Figure 10 is a schematic of the telescope arrangement. Figure 10(a) shows a direct image of the light source with the heater off. It should be pointed out that, even with no artificial turbulence introduced, the diameter of the source cannot be accurately ascertained from the diameter of the photographic image, since the latter depends on the exposure and is, furthermore, diffraction-limited. Figure 10(b) shows the same image with the heater on. An additional image enlargement due to turbulence is quite evident; the enlargement is asymmetric because

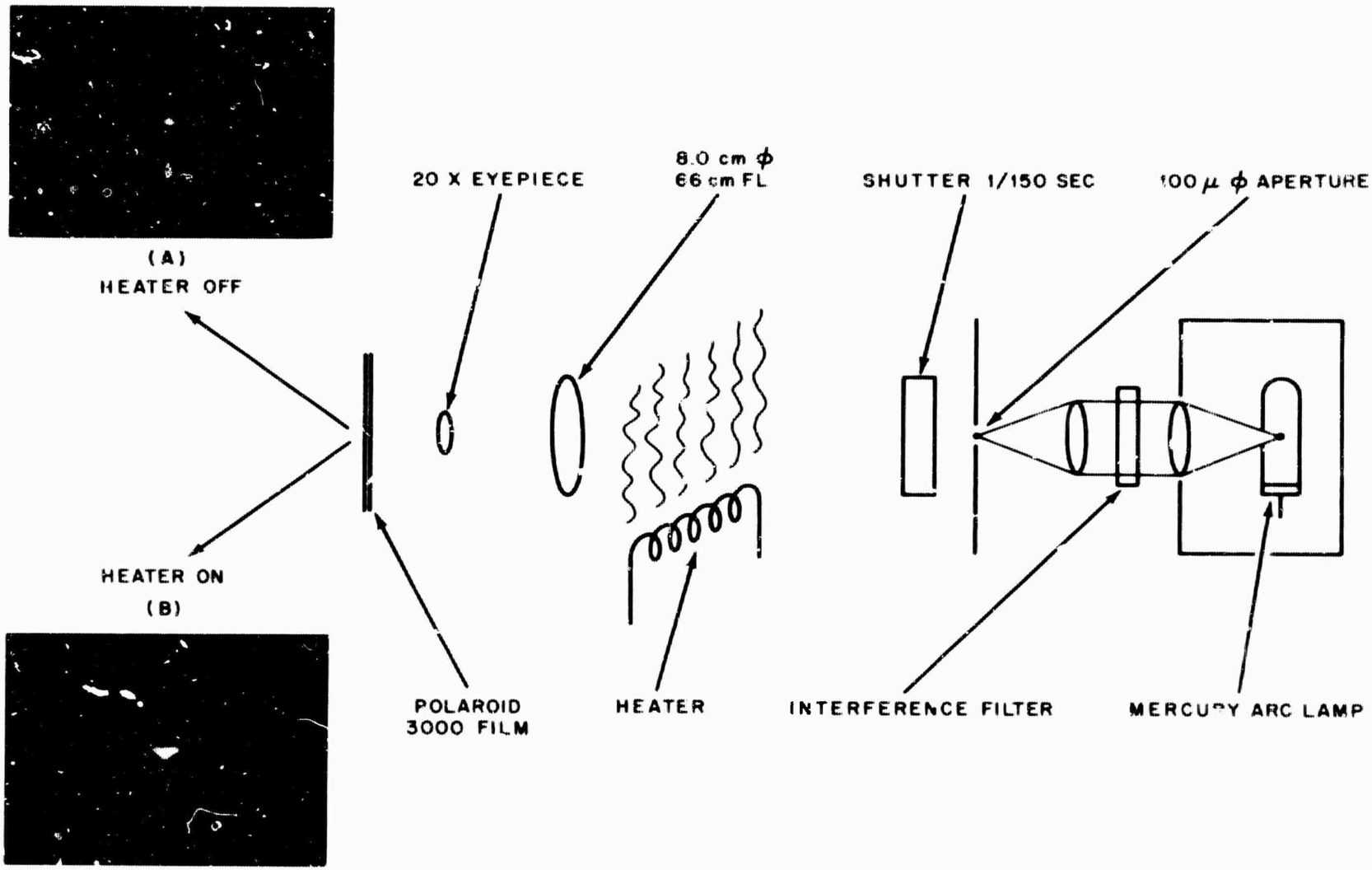

Figure 10. Effect of Turbulence on Source Image

of the vertical motion of the heated air. The visual impression is one of rapid image motion predominantly at right angles to the direction of the air currents.

The Fizeau interferometer experiments described so far made use of sets of diffracting apertures with holes separated by discrete distances. A new component was designed and fabricated to allow the space between the apertures to be changed continuously. A cable was attached to the screw on the device so the operator can change the distance between the apertures while viewing the fringes. The design, shown in Figure 11, also maintained identical distances between each diffracting aperture and the optical axis. The new component was placed on a 4 ft x 6 ft granite table that rested on the floating floor of a recently completed building and provided a relatively vibration-free support. The table is flat to within 0.0006 in. The light source, placed at a distance of 2,054 cm from the interferometer, consisted of a pinhole illuminated incoherently with filtered light from a mercury arc source.

In a typical experiment the pinhole light source was 0.0685 cm in diameter. With the variable diffracting apertures positioned close to a lens with a 26-in. focal length and a 3-in. diameter, fringes were observed in the focal plane (using a low power microscope) for aperture separations less than about 2.3 cm. Near 2.3 cm the fringe visibility approached zero. Using the symbols of Chapter 2, we find the calculated source angle, α_o, is then given by:

$$\alpha_o = \frac{1.22\lambda}{S_{ext}} = \frac{1.22 \times 5461 \times 10^{-4}}{2.3} = 2.9 \times 10^{-5} \text{ rad} .$$

The actual angle subtended by the source was $\alpha = \frac{0.0685}{2054} = 3.3 \times 10^{-5}$ rad. The discrepancy is likely to be the result of some uncertainty in the visual estimate of zero visibility. This estimate is made difficult by the relatively high spatial frequency of the fringes, and is aggravated by minor air currents that always tend to be present in the air path between the source and the interferometer. These air currents may be caused by the air conditioning system and by thermal gradients existing within the laboratory.

The factors mentioned above also prevent an accurate measure of fringe contrast to be obtained by means of photographs for which the exposure has to be longer

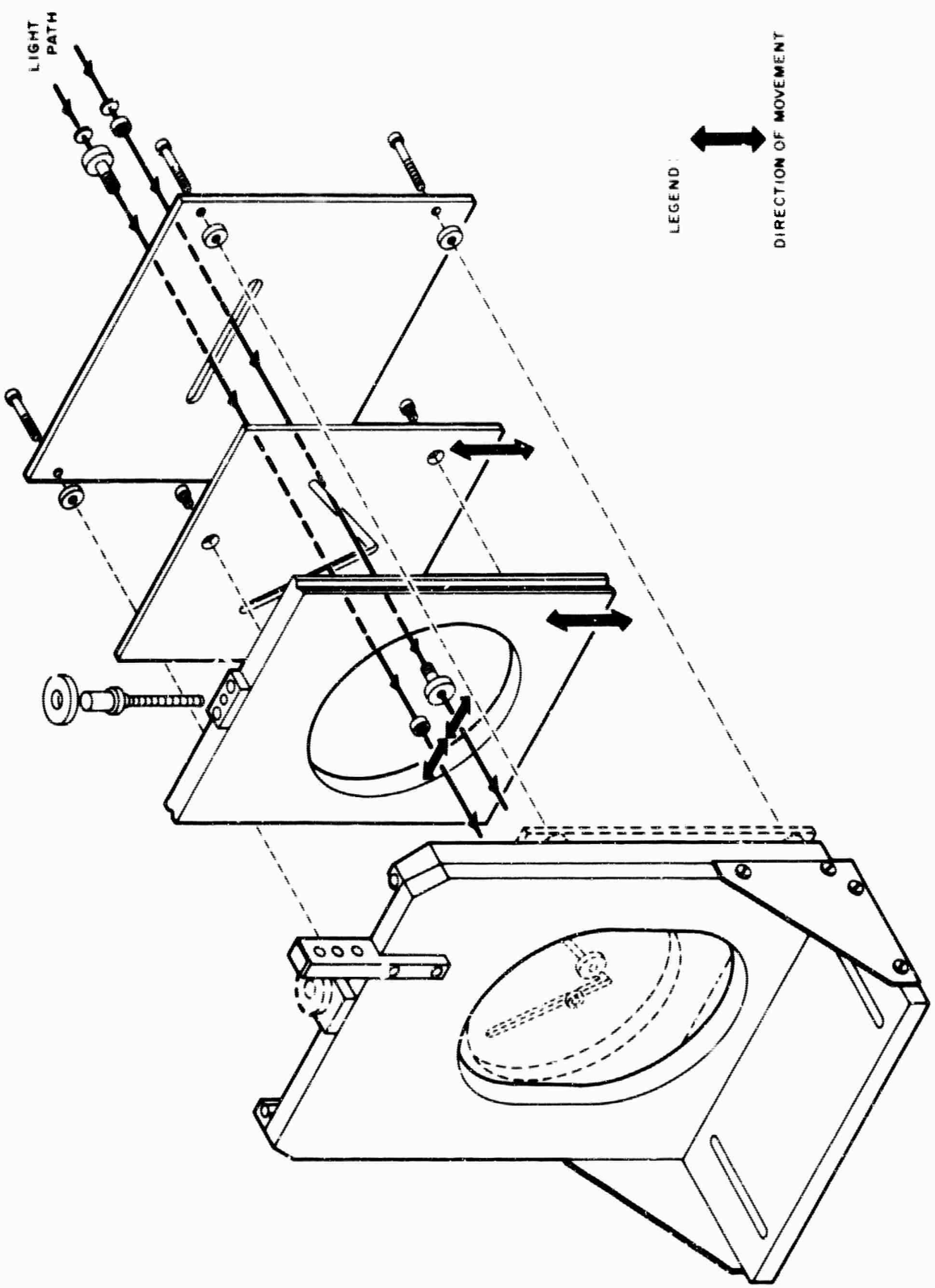

Figure 11. Modified Tech/Ops Y Carriage for Fizeau Experiment

than a fraction of a second. In the Fizeau arrangement described, the fringe spacing rather than the lens diameter sets a limit to the smallest angular source diameter that can be determined.

MICHELSON STELLAR INTERFEROMETER

DESIGN PARAMETERS

The Fizeau setup was subsequently replaced by a Michelson arrangement as shown in Figures 12 and 13. The inner mirrors consisted of a small, right-angle prism aluminized on two sides. The outer mirrors were flat to within 1/8 wavelength; one of them was attached to a mechanical stage that could be moved accurately to vary its spacing from the optical axis. The diffracting apertures (visible in Figure 13) were 2.5 mm in diameter and 1 cm apart. The close spacing provided a relatively wide fringe spacing that eliminated the need for high magnification in the viewing microscope. The fringe spacing is, of course, determined solely by the separation of the diffracting apertures and is unaffected by the separation of the outer mirrors. Much greater coherence intervals can therefore be sampled than by the Fizeau arrangement.

A possible disadvantage of the Michelson arrangement is the extreme precision with which the mirrors have to be aligned to obtain exact overlap of the diffraction discs. Furthermore, because of the short coherence length of the filtered-mercury arc light (coherence length = $c/\Delta\nu \cong 0.001$ in. for an assumed bandwidth of 100 Å), the mirrors have to be accurately centered around the optic axis to make the two light paths almost equal. Even for narrower bandwidth, near path equality is necessary to obtain the highest possible fringe contrast. To duplicate Michelson's stellar interferometer would, therefore, require either extreme precision in the mirror-moving mechanism or appropriate compensating devices to ensure overlap of the diffraction images and equalization of path length. (Michelson used the latter alternative.)

A more expedient solution, one not available to Michelson, of course, was to set up the mirrors at a given separation smaller than the coherence interval (in the mirror plane) of the radiation emitted by a given source so as to produce fringes. Then the size of the source was increased until the fringes disappeared. The

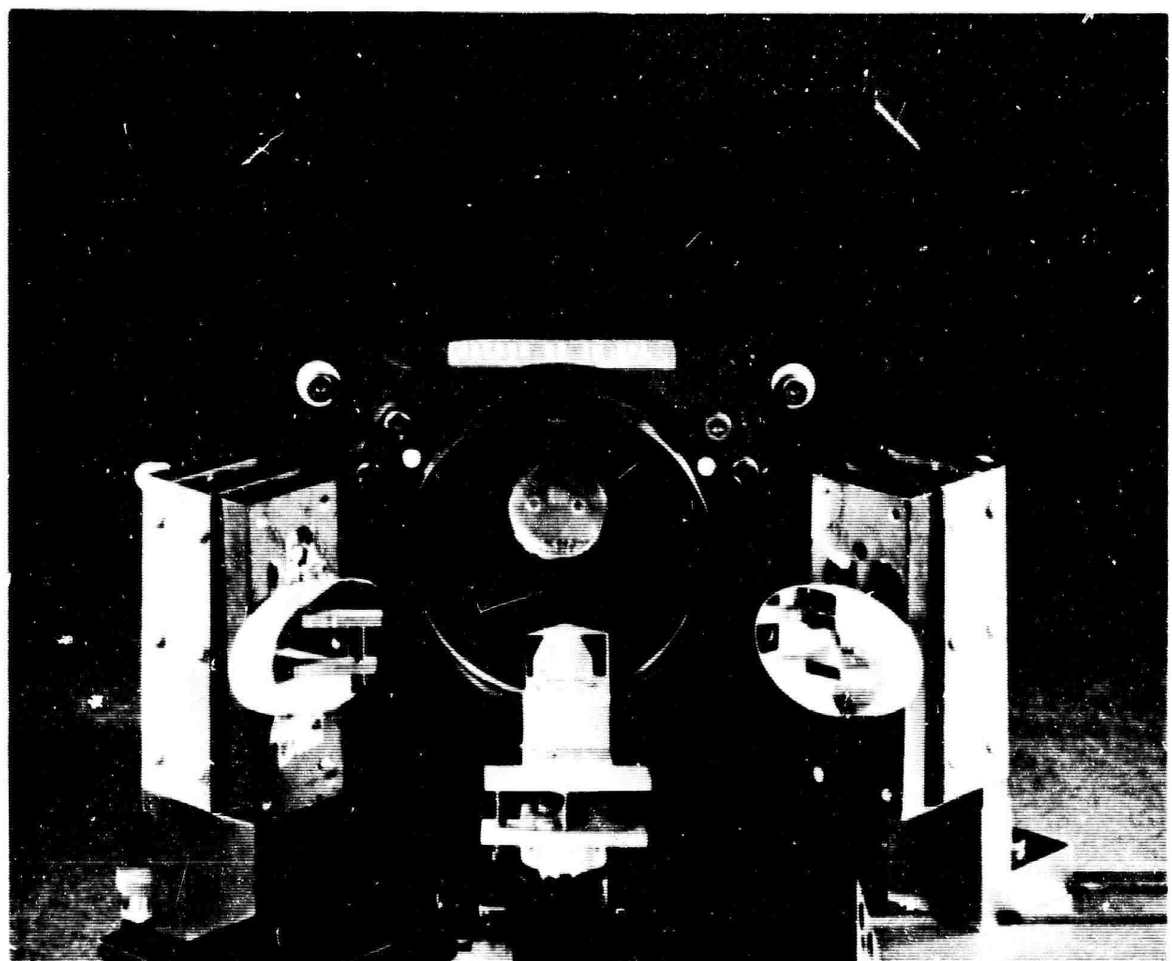

Figure 12. Close-up of Lens and Mirrors in Michelson Interferometer

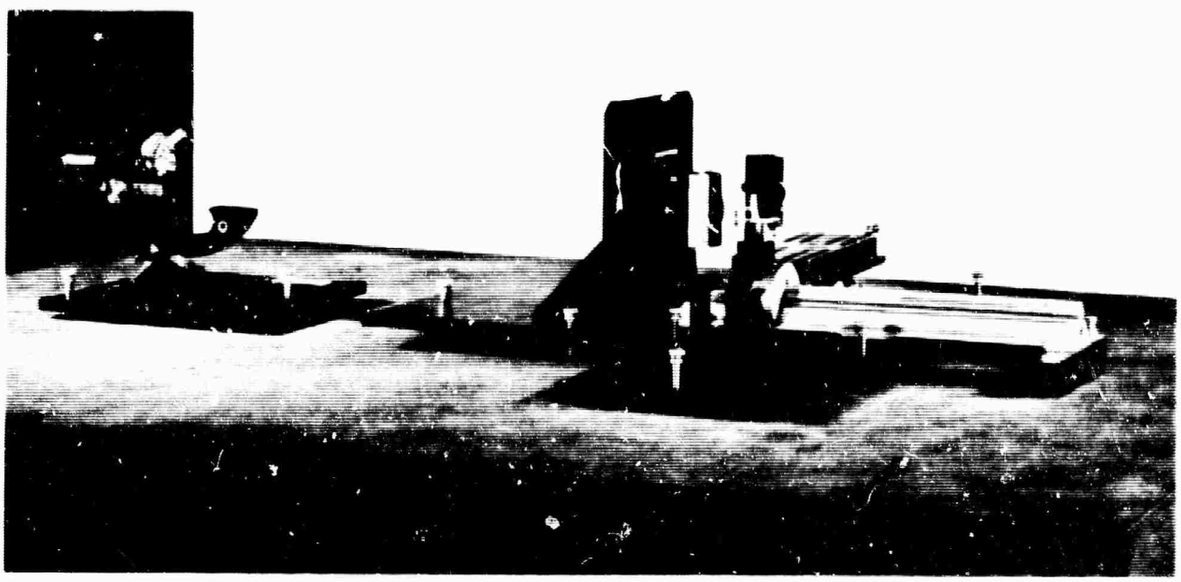

Figure 13. Side View Michelson Interferometer

variability of the source size was achieved by illuminating a 120-μ diameter aperture with a mercury source and by producing an aerial image of this aperture with a low-power microscope lens. By varying the distance between the lens and the aperture, the size of the aerial image was varied accordingly. The difficulty of staying within focus was also eliminated by keeping the mirror separation constant. Preliminary measurements were made with the outer mirrors about 11 cm apart. At this separation the fringes disappeared when the source subtended 6.1×10^{-6} rad. This is in good agreement with theory.

In the Michelson interferometer, any movement of the outer mirrors is accompanied by a shift in the image position. The calculations given below show that a movable mirror system imposes restrictions on source size and distance. Because of this (and other considerations as discussed above), a fixed mirror system was adopted.

Image Shifting

If the interferometer is treated as an array of mirrors, the virtual image of the source due to the mirror system may be used as a secondary source. A schematic of such an arrangement with two different mirror positions is shown in Figure 14. In this diagram:

① represents an outer position of the movable mirror

② represents the innermost position of the movable mirror

③ represents the stationary position of the inner mirror

O represents the object

O_1 represents image of O through the mirror system ① and ③

O_2 represents image of O through the mirror system ② and ③

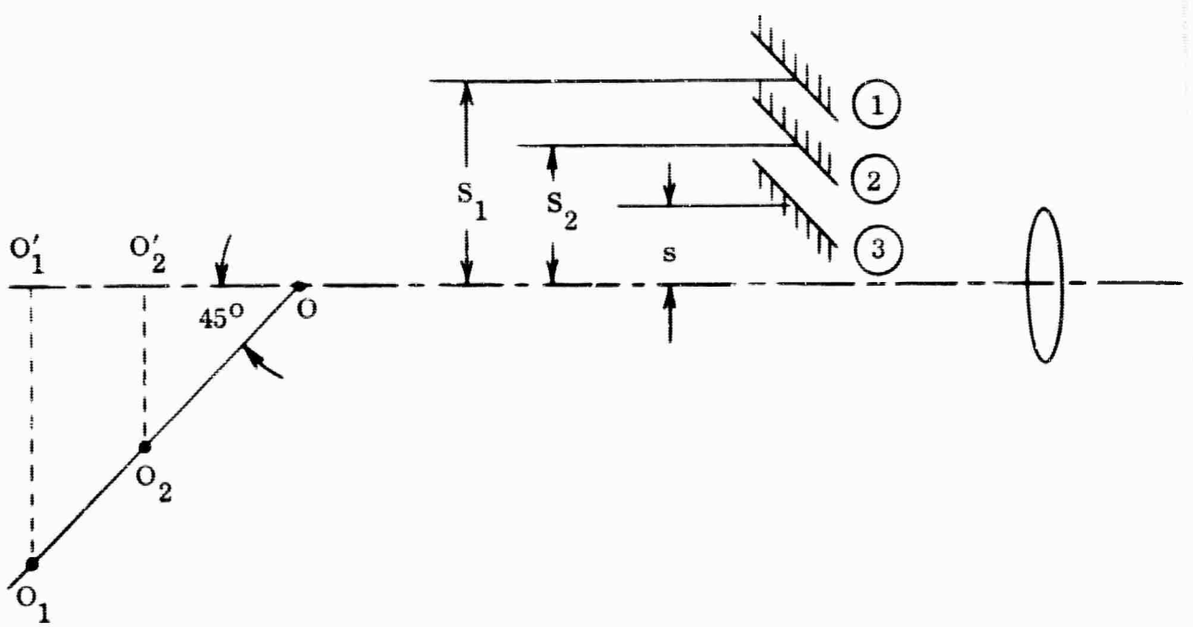

Figure 14. Design Parameters for Michelson Interferometer (Schematic)

It is easily seen from the geometry of the figure that

$$O O'_1 = S_1 - s \text{ and } O O'_2 = S_2 - s \quad .$$

If

ξ = object distance

η = image distance

f = focal length of lens .

Then using the Gaussian lens formula, we find

$$\Delta\eta_{\text{long.}} = \eta_1 - \eta_2 \sim \frac{(S_1 - S_2)\, f^2}{\xi_1^2} \tag{27}$$

where it has been assumed that

$$\xi_1 >> f >> 1; \; \xi_1 \sim \xi_2 \quad .$$

This expression gives the image shift along the axis. To find the off-axis shift perpendicular to the axis, the linear magnification of the system is used. If h_s represents the image height then

$$\Delta\eta_{\text{lat}} = h_2 - h_1 = \frac{f}{f - \xi_1}(S_1 - S_2) \quad . \tag{28}$$

Depth of Focus

The three-dimensional intensity distribution in the error-free diffraction pattern of a circular aperture exhibits a tubular structure[13,14] and, hence, a certain amount of defocussing can be tolerated. The distribution of intensity is

shown in Figure 15, which is adapted from Linfoot and Wolf;[13] the parameters u and v are defined as follows:

$$u = \frac{2\pi s^2}{\lambda f^2}\Delta f, \quad v = \frac{2\pi sr}{\lambda f} \tag{29}$$

where s is the radius of the aperture, f radius of curvature of the converging spherical wave, Δf the out-of-focus distance, λ the wavelength, and r a polar coordinate of the field point. Figure 15 shows that the diameter of the Airy disc is not sensibly changed for a defocussing of $u = 2\pi$, since the 0.1 isophote is almost horizontal. Using this amount of defocussing as the limiting condition and substituting for u in Eq. (29), we obtain

$$\Delta f = 4\lambda (F^{\#})^2 \ . \tag{30}$$

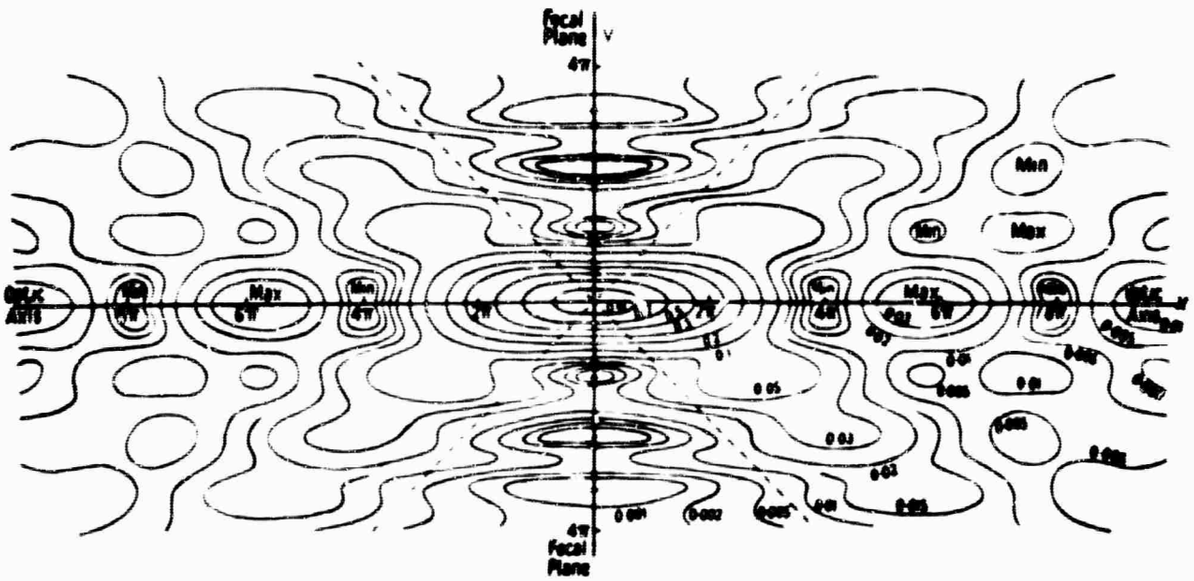

Figure 15. Distribution of Intensity in Error-Free Diffraction Pattern (from Taylor and Thompson[14])

Demanding that

$$\Delta\eta_{\text{long.}} < \Delta f$$

and combining Eq. (27) and (30), we see that

$$s^2 < \frac{\lambda \xi_1^2}{(S_1 - S_2)} \quad . \tag{31}$$

Thus if this inequality is satisfied, a change of focus will not have to be made when the measurements are performed. Equation (31) is plotted in Figure 16 with S_1 as the ordinate and ξ_1 as the abscissa. The values s = 3.5 cm and S_2 = 7 cm, used to plot Figure 16, are experimentally realizable for this arrangement.

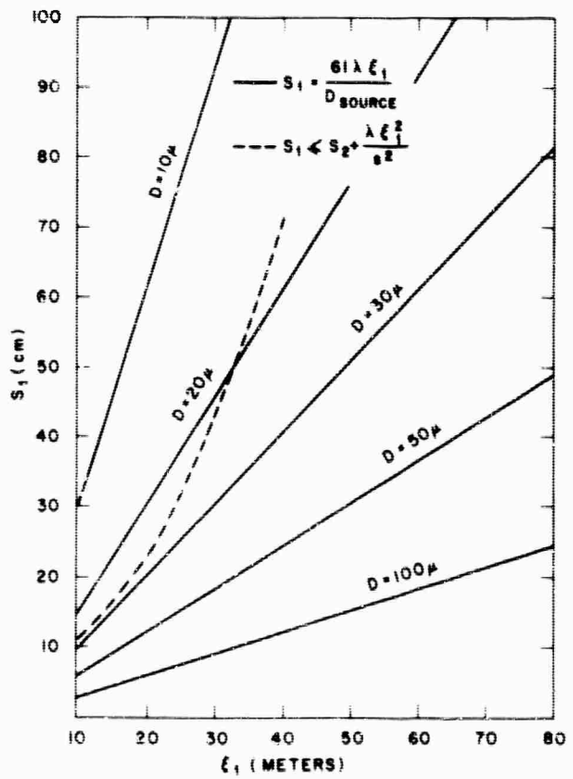

Figure 16. Design Parameters for Michelson Stellar Interferometer

Source Diameters

Knowledge of the size of the incoherent sources that will be useful for a particular experiment is also valuable. The van Cittert Zernike theorem enables one to calculate the equivalent incoherent source that gives a particular visibility curve in the plane of the movable mirrors. If the separation of the correlation points (i.e., the outer mirrors) is such that there is complete incoherence (i.e., the first zero in the visibility curve), then the diameter of the incoherent circular source giving rise to the particular visibility curve is given by

$$D_{source} = \frac{0.61\lambda\xi_{1,2}}{S_1} \quad . \tag{32}$$

Equation (32) is also plotted in Figure 16 for different values of Γ_{source}. From Figure 16 the useful source diameters are those below the curve satisfied by Eq. (31). A similar set of curves may be drawn for any position of the inner mirrors.

EXPERIMENTAL PROBLEMS

In the preceding section, it was shown that it was more advantageous to change the size of the source than to change the mirror separation in the Michelson interferometer. The source size was changed by illuminating a small aperture with a mercury source and by producing an aerial image of this aperture with a low-power microscope lens. By manually varying the distance between the lens and the aperture, the size of the aerial image could be varied. In practice, this arrangement required two operators, one to observe the interference fringes, the other to move the microscope objective. Because the distance between the operators was considerable, communication was somewhat awkward. Furthermore, it was soon apparent that the operator observing the fringes had to have more direct control of the source size.

A servo system, shown in Figure 17, was therefore designed and constructed. It consisted of a hand-cranked servo generator mechanically coupled to a revolution counter. The generator was kept within easy reach of the operator and was electrically connected to the servo motor. The servo motor moved the microscope

BLANK PAGE

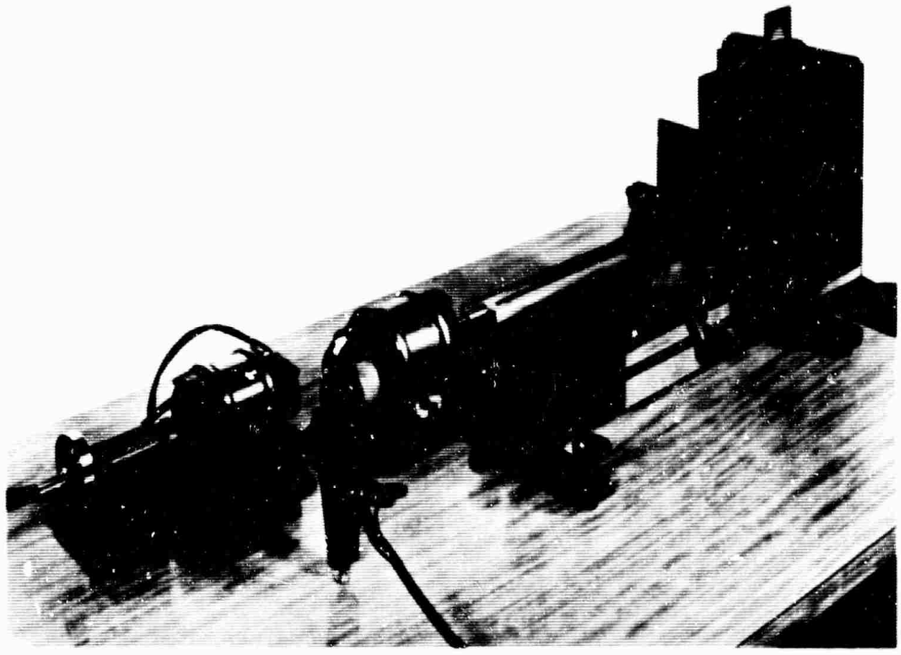

Figure 17. Servo System to Vary Source Size

objective along the optical bench via a finely threaded screw. One turn of the crank corresponded to a movement of 2.5×10^{-2} cm. The number appearing on the revolution counter could therefore be correlated with the object distance; i.e., the distance between the aperture and the back focal plane of the microscope objective. The nonlinearity that exists between the movement of the five power objective (focal length f = 2.75 cm) and the magnification of the aperture is shown in Figure 18. The curve shows that for magnifications greater than unity a small movement of the objective will bring about a relatively large change in magnification and hence in source size. The system should therefore be used for magnifications less than unity if sensitive control of source size is desired.

The servo system performed very well and eliminated the unsatisfactory aspects of the manual operation. However, other difficulties in the determination of source size by the disappearance of interference fringes became apparent. These difficulties are discussed below.

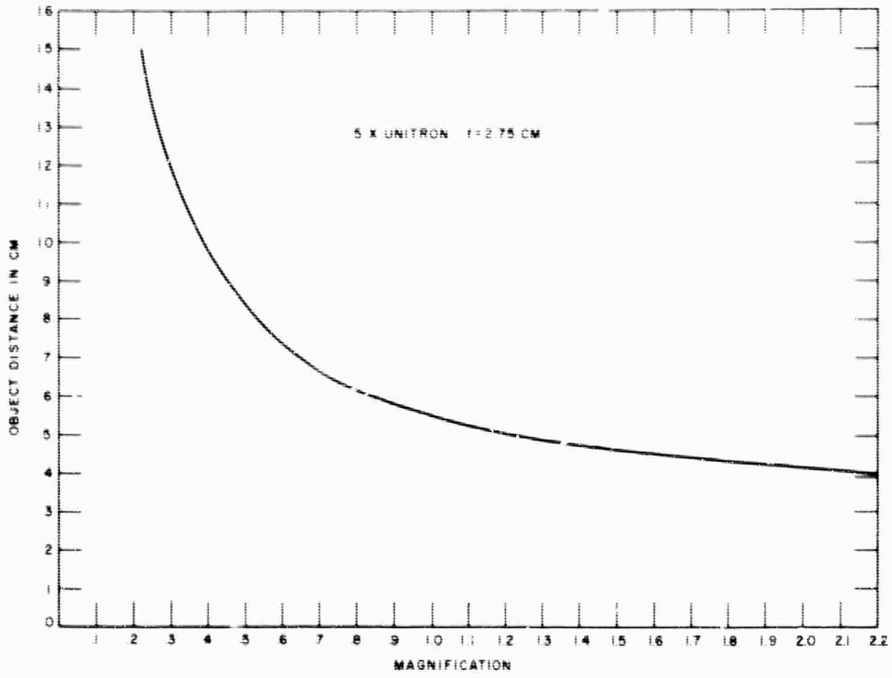

Figure 18. Magnification as a Function of Object Distance

LOW LIGHT LEVELS

The low light levels encountered in the focal plane of the telescope are the result of the small angle subtended by the light source to be measured (of the order of microradians) and of the small diameter of the diffracting apertures. Because of the low light levels, any photographic record of the interference fringes would require long exposure times. Since in practice the fringes are not completely static, exposure times of long duration would record only a blurred or distorted diffraction disc of the diffracting apertures.

Only visual observations of fringe contrast could therefore be made. Visual observations, of course, have severe limitations. Among these are:

1. Differences in visual acuity between different observers
2. Dependence of contrast discrimination on light level and degree of dark adaptation of the eye
3. Inability of the eye to judge contrast of rapidly moving fringes
4. Difficulty in comparing fringe contrast under different situations because of poor visual memory.

Photoelectric detection of interference fringes could no doubt overcome these disadvantages. Photometric calculations pertaining to the present system are given below.

PHOTOMETRIC CONSIDERATIONS

To calculate the illuminance of the diffraction pattern, we first calculate the illuminance E_1 at the apertures of the interferometer. It can be shown that E_1 = B x solid angle subtended by source, where B is the luminance of the source. For the 100-W Osram Mercury Lamp used, $B = 4.4 \times 10^{3}$ lu sr^{-1}. A typical solid angle subtended by the source during recent experiments is 5×10^{-6} rad. This is equivalent to 2.0×10^{-11} sr. Therefore, $E_1 = 8.8 \times 10^{-8}$ lu cm^{-2} before filtering. If a suitable interference filter is used to isolate the 5460-Å mercury line, the illuminance will be reduced by a factor of about 4; hence $E_1 = 2.2 \times 10^{-8}$ lu cm^{-2}.

The illumination E of the diffraction disc depends on E_1, diameter, and the f-number of the system. The f-number of the present system is the ratio of the effective focal length (nominal focal length of objective times magnification of eyepiece = 660 cm) and the diameter of the diffracting apertures (0.33 cm). Therefore, the f-number is 2×10^{3}.

The diameter of the diffraction disc is then given by

$$D = 2 \times 1.22 \times \lambda \times \text{f-number}$$

$$= 2.44 \times 0.54 \times 10^{-4} \times 2 \times 10^{3} = 0.26 \text{ cm}$$

and its area is 5.4×10^{-2} cm^2.

The two diffracting apertures have a total area of 0.175 cm^2; they therefore collect $2.2 \times 10^{-8} \times 0.175$ lu $= 3.9 \times 10^{-9}$ lu. About 80% of this (3.1×10^{-9} lu) falls on the 5.4×10^{-2} cm^2 area of the diffraction disc, resulting in an illuminance of 5.8×10^{-8} lu cm^{-2}. In terms of watts (assuming 685 lu W^{-1}) this is equivalent to 8.5×10^{-11} W cm^{-2}. Photographic film such as Kodak Pan X needs about 2×10^{-8} W-sec cm^{-2} for a density of 1 above fog. Therefore, the disc mentioned

above would have to be exposed for about 230 sec to be recorded on film. This is not practical, of course, since the fringes can be expected to move during such a long time interval.

FADE-OUT OF FRINGES

Even with no artificial turbulence introduced in the path between the interferometer and the source, the fringes, especially near fringe extinction, in many instances faded in and out of the field of view. This phenomenon did not seem to be caused by air turbulence, since it persisted whether the air-conditioning fan was operating or not. The most likely cause, especially in view of evidence found in the last part of this report period, is the intensity variation across the illuminated source aperture. This fading out of the fringes could result from a minor spatial instability of the mercury arc, from slight vibrations between the lamp housing and the illuminated source aperture, or from the effect of a convection current caused by the red-hot mercury lamp. In any case, the fading often makes the visual determination of zero fringe visibility very difficult. Photoelectric fringe detection would no doubt help to pinpoint the cause of the fade-outs and perhaps to overcome them.

EFFECT OF SOURCE NON-UNIFORMITY

The formula for the angle subtended by the source, $\alpha = 1.22\,\lambda/d_{ext}$ (where λ is the wavelength and d_{ext} the separation of the diffracting apertures at which extinction occurs), is based on an "ideal" circular source uniformly and incoherently illuminated. Most light sources encountered in practice, however, are: (a) not circular but uniformly illuminated, (b) circular but not uniformly illuminated, or (c) not circular and not uniformly illuminated. In the servo system described previously, for instance, even if the original aperture had been evenly illuminated, the microscope lens used to produce the secondary image would have contributed some unavoidable fall-off of intensity toward the edges of the disc. Furthermore, because of the condenser lenses, some coherence exists across the aperture. Interferometric determinations in which $\alpha = 1.22\,\lambda/d_{ext}$ is used for the calculation of source size will therefore contain errors, the magnitude of which depends on how far the actual source deviates from the ideal. This has been borne out by a number of measurements.

Toward the end of the report period, an attempt was made to (1) approach a uniform light distribution by eliminating the microscope lens between the source aperture and telescope, and (2) investigate the relationship between source shape, source size, and uniformity of illumination versus d_{ext}. The method was direct but fairly laborious: A "pinhole" about 60 μ in diameter was punched into brass shimstock. This source aperture was set up on an optical bench and illuminated by a mercury arc. It was then photographed through a microscope objective onto Pan X film. Figure 19(a) is an enlargement of the negative and Figure 19(b) is a recording of the negative made by the ISODENSITRACER$_{tm}$.* The recording, together with the characteristic curve for the film, made it possible to assign relative luminance values to different regions of the aperture. The microscope camera was then removed and the mirrors of the interference telescope set so that fringes were obtained with the source apertures toward the end of the bench farthest from the telescope. While one operator slowly moved the source aperture toward the telescope, another watched the interference fringes. At the same time, as the source came closer, the eyepiece had to be moved away from the telescope lens to keep the fringes in focus The fringes disappeared at a mirror setting of d = 22.2 cm and a distance of the source aperture of 1430 cm. This corresponds to a source size of 41 μ, with a circular incoherent source of uniform intensity assumed.

The isodensity recording indicates a characteristic source size of 74 μ with about one fourth the source having an intensity of about one half the remainder of the source. At first glance it would appear unlikely that this distribution could so affect the zero point that it would differ by about a factor of two from the uniform circular source. A simple one-dimensional calculation, however, gives us a different perspective. Consider the intensity distribution in Figure 20.

*The ISODENSITRACER$_{tm}$ developed by Technical Operations Research provides a quantitative, two-dimensional density map of film-recorded images. Repeated, stepped scans of the transparency furnish the complete map of all image points, generating equidensity contours. The printout utilizes one pen with a three-symbol code to unambiguously establish positive or negative density gradients. Absolute density at any point can be found from the density at one given point and the contour interval step.

Figure 19(a). Photomicrograph of Source Aperture

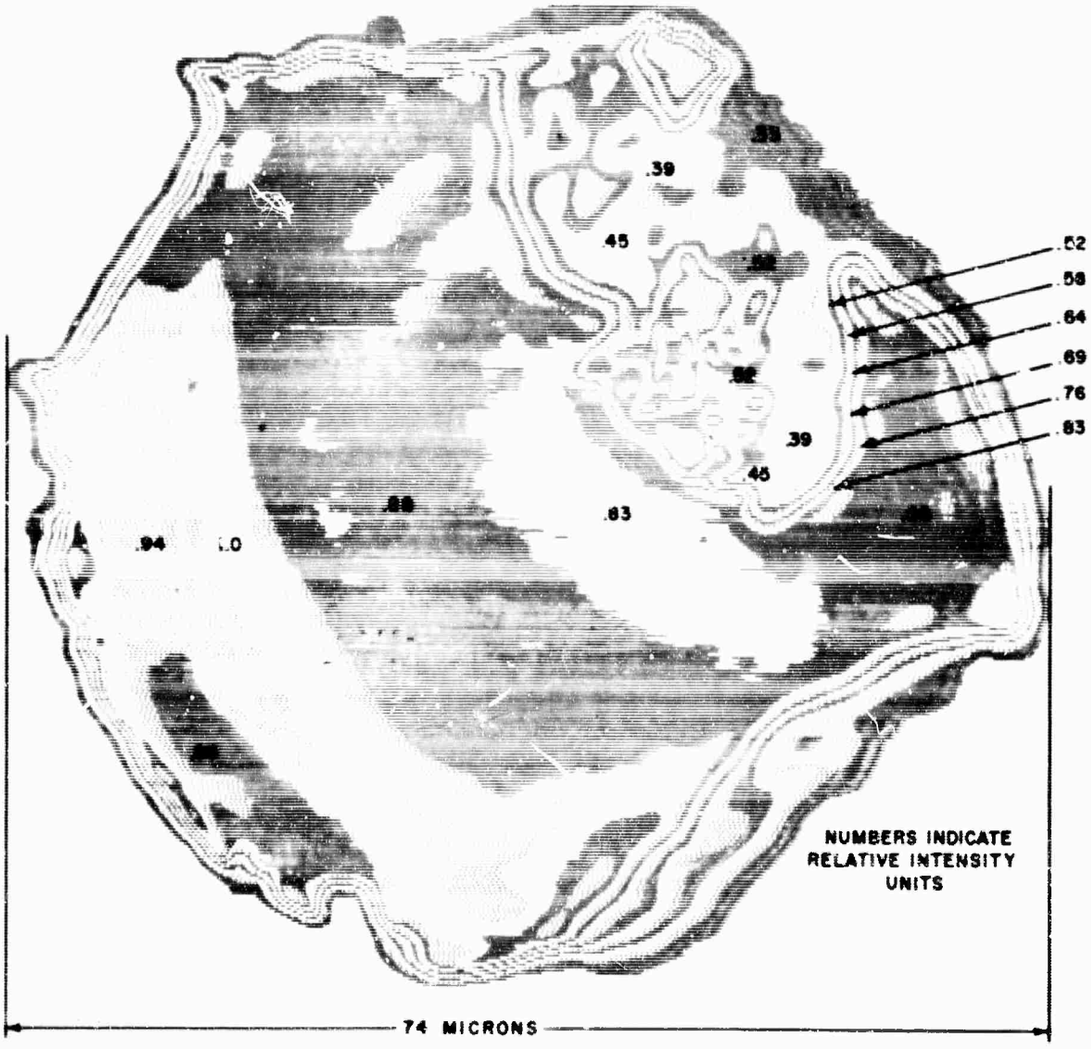

Figure 19(b). Isodensity Recording of Photomicrograph

If the zero point corresponding to this distribution occurs at the point $x = b_o$ for $\beta = 1$, then it occurs at the point $x_o = 2b_o$ for any value of $\beta < 1$ not just $\beta = 0$. To be sure, if β is close to 1, the visibility approaches zero at $x = b_o$, but does not equal zero, and if the measuring apparatus is not very sensitive, one may fail to notice the decrease in visibility at the point $x = b_o$ and proceed to the point $x = 2b_o$.

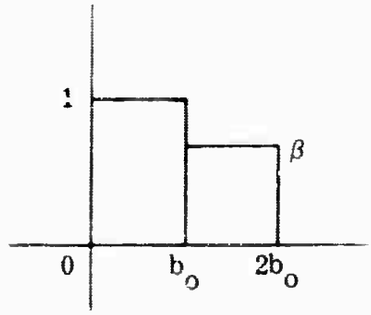

Figure 20. One-Dimensional Intensity Distribution

To avoid this pitfall one must plot visibility as a function of separation to make sure that no significant dips in the visibility curve are overlooked.

CONCLUSIONS

To obtain accurate interferometric measurements of source size, the light distribution across the source has to be taken into account. Only if the distribution is very close to uniform can the formula $\alpha = 1.22\lambda/d_{ext}$ be used.

Visual interferometric determinations of source size have many shortcomings that could be overcome by photoelectric fringe detection.

CHAPTER 4

ANALYSES OF FOLDING AND FIZEAU INTERFEROMETERS

INTRODUCTION

This chapter concerns the work performed by Technical Operations Research under Contract No. P.O. No. 11241-A-1 during the period from 4 to 30 November 1964. Experiments were conducted to compare analytically the performance of the standard Fizeau interferometer and the folding interferometer.

Fizeau interferometers have been very useful in measuring the angular diameters of astronomical objects. Currently, interest has been expressed in the utility of these interferometers for measuring the angular diameters of nearby man-made objects . Recently, another type of interferometer was proposed by Mertz[7] to also perform these measurements. It was hoped this instrument would not be subject to some of the limitations of the Fizeau interferometer. The performance of the two types of interferometers are compared to discover if the folding interferometer proposed by Mertz is more suitable for certain angular diameter measurements.

MATHEMATICAL ANALYSIS OF THE FOLDING INTERFEROMETER

We shall begin with a general mathematical description of the operation of the wave-front folding interferometer and then analyze it as a measuring device. The wave-front folding interferometer differs from the traditional interferometer in that the amplitude of the incoming wave front is halved, one half is folded with respect to the other, and the original and the mirror image are recombined to form interference fringes (see Figure 21). In addition, by tilting a mirror, a fixed amount of vertical shear may be introduced. The reason for this will be seen presently.

Mathematically, the incoming wave front may be represented as

$$e^{ik(\alpha x + \beta y)} \tag{33}$$

and its mirror image with shear $2\beta_o$ by

$$e^{ik(-\alpha x + (\beta - 2\beta_o)\, y)}\ , \tag{34}$$

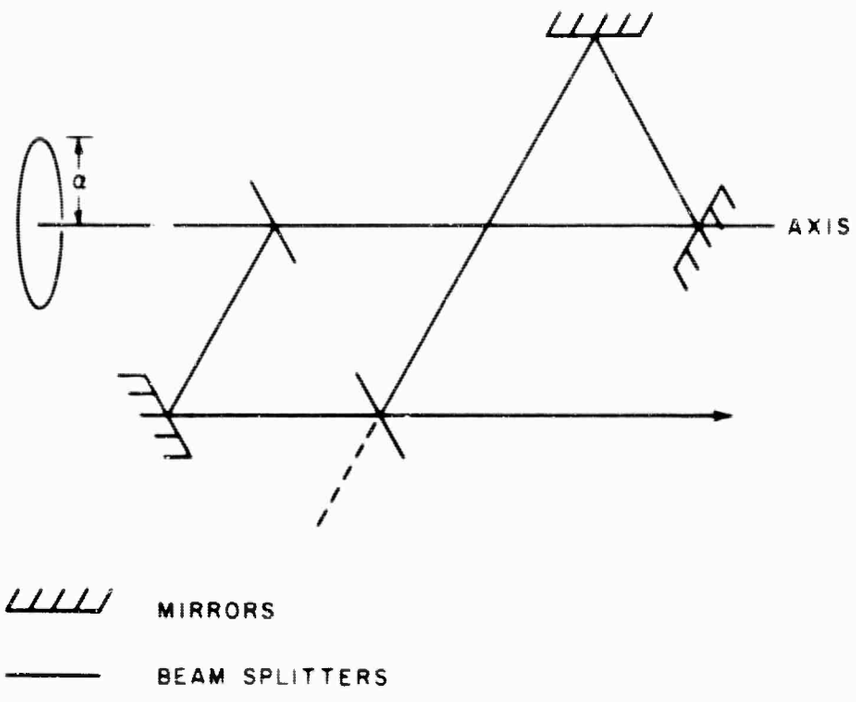

Figure 21. Representation of the Wave-Front Folding Interferometer

where α and β are the angular dimensions in object space, and x and y are the dimensions in image space (see Figure 22). The amplitude of the recombined wave front is given by

$$A(x, y) = e^{ik(\beta - \beta_o)\, y} \left[e^{ik(\alpha x + \beta_o y)} + e^{-ik(\alpha x + \beta_o y)} \right] \tag{35}$$

and the intensity distribution by

$$\begin{aligned} I(x, y) &= |A|^2 = 4 \cos^2 k(\alpha x + \beta_o y) \\ &= 2 \left[1 + \cos 2k(\alpha x + \beta_o y) \right] . \end{aligned} \tag{36}$$

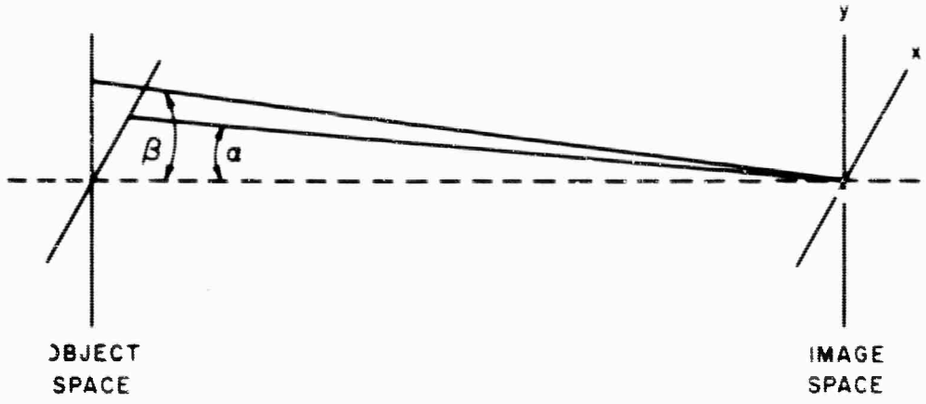

Figure 22. Relation of Object to Image Planes in the Folding Interferometer

Since this corresponds to the impulse response of a point object at some angular displacement α, the image intensity distribution for any object distribution $f(\alpha, \beta)$ is given by the superposition integral

$$I(x, y) = 2 \iint f(\alpha, \beta) \left[1 + \cos 2k(\alpha x + \beta_o y) \right] d\alpha \, d\beta \quad . \tag{37}$$

In general, this may be related to the Fourier transform of the object distribution by writing

$$I(x, y) \cong N + \cos 2k\beta_o y \int \cos 2k\alpha x \, d\alpha \int f(\alpha, \beta) \, d\beta$$

$$- \sin 2k\beta_o Y \int \sin 2k\alpha x \, d\alpha \int f(\alpha, \beta) \, d\beta \quad , \tag{38}$$

where N is a constant. If we identify $\int g(\alpha) \cos 2k\alpha x \, d\alpha$ (where $g(\alpha) = \int f(\alpha, \beta) \, d\beta$) with the Fourier cosine transform $\tilde{F}_c$ of an average distribution and $\int g(\alpha) \sin 2k\alpha x \, d\alpha$ with the sine transform $\tilde{F}_s$, we have

$$I(x, y) = N + \tilde{F}_c(x) \cos 2k\beta_o y - \tilde{F}_s(x) \sin 2k\beta_o y \quad . \tag{39}$$

If the object distribution is an even function of α, i.e.,

$$f(-\alpha, \beta) = f(\alpha, \beta) \quad ,$$

this relation becomes

$$I(x, y) = N + \tilde{F}(x) \cos 2k\beta_o y \quad . \tag{40}$$

Without shear in the system, one can thus directly view the average one-dimensional Fourier transform of a symmetrical object. For a nonsymmetrical object, the relationship is given by Eq. (39). To find $\tilde{F}_c$ we measure $I(x,$ for $\beta_o = 0$, and to find $\tilde{F}_s(x)$ we measure $I(x, y_1)$ for $2k\beta_o y_1 = \pi/2$. If the object is truly one dimensional, the instrument allows the determination of the complete Fourier transform of the internally distributed object.

Figure 23 shows some of the interference patterns for various configurations of point objects. Note that the shear tends to rotate the pattern.

At this point, since we have the impulse response for a point object, let us derive a criterion for the resolution of two-point objects. The intensity distribution for two-point objects separated an angular distance 2d whose midpoint is at α_o is given by

$$I(x, y) = 2 \left[2 + \cos 2\bar{k} \left\{ (\alpha_o + d)\, x + \beta_o y \right\} + \cos 2\bar{k} \left\{ (\alpha_o - d)\, x + \beta_o y \right\} \right] \tag{41}$$

or, simplifying,

$$I(x, y) = 4 \left[1 + \cos 2\bar{k} (\alpha_o x + \beta_o y) \cos 2\bar{k} dx \right] \quad . \tag{42}$$

If in this expression we consider $\cos 2\bar{k}dx$ as an envelope from which measurements can be made, we can establish the necessary resolution limits.

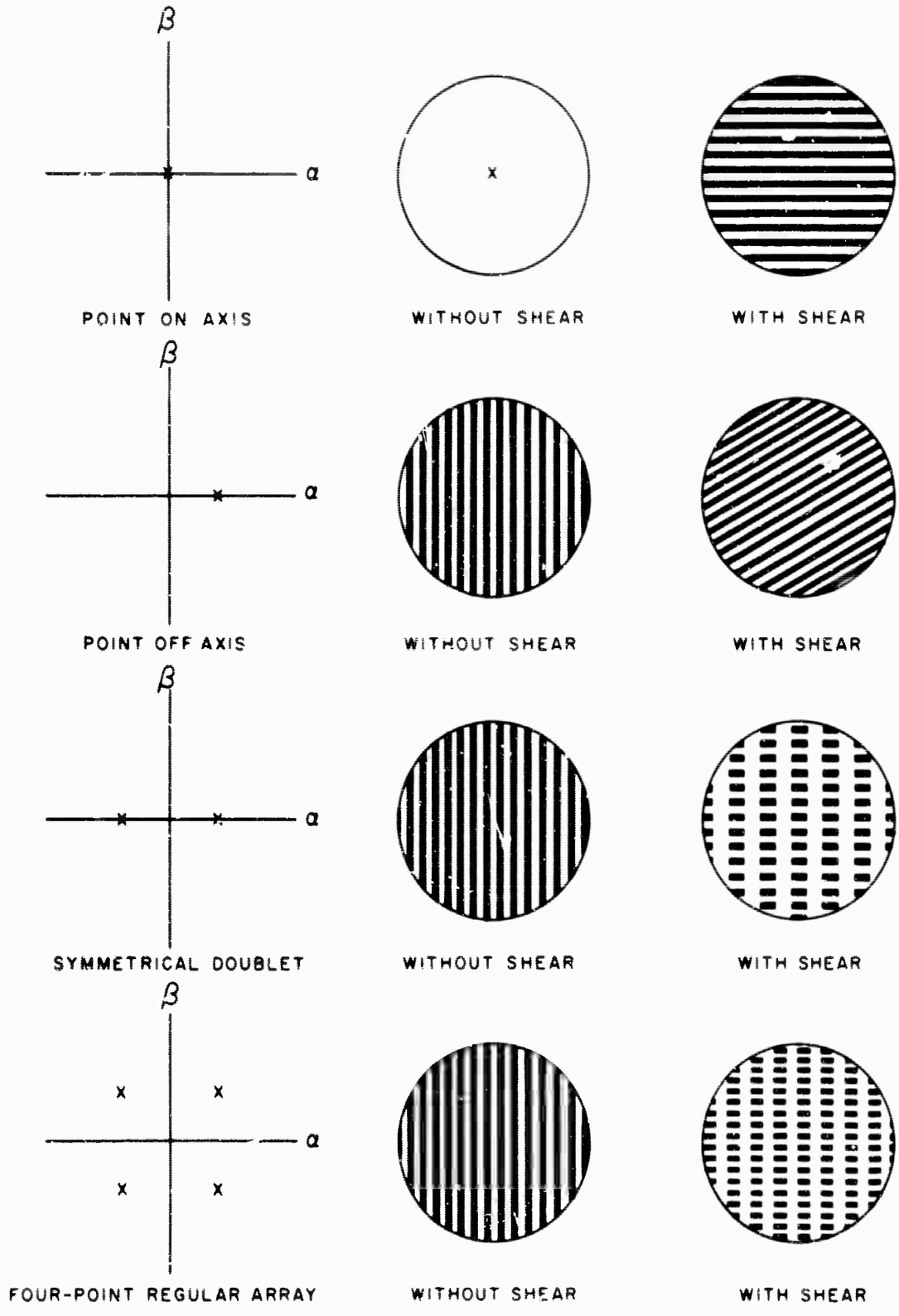

Figure 23. Interference Patterns

First, the minimum separation is given when one cosine peak just fills the aperture, i.e., for $\alpha = \lambda/4a$. With sufficient shear and small angular displacement in the system so that the fringes are almost dependent only on y, there is no limit on d other than that of the measuring device.

Next, consider the case where a single-point object becomes resolvable. From Eq. (37), a square, regularly oriented, of width 2b would yield

$$I(x,y) = 2 \int_{-b}^{b} \int_{-b}^{b} \left[1 + \cos 2\bar{k}(\alpha_o x + \alpha x + \beta_o y) \right] d\alpha \, d\beta \quad , \tag{43}$$

where α_o is some angular displacement, introduced as the most general case. On integration, we find

$$I(x,y) = 8b^2 \left[1 + \cos 2\bar{k}(\alpha_o x + \beta_o y) \operatorname{sinc} 2\bar{k}bx \right] \quad . \tag{44}$$

As shown in Figure 24(b), the sinc envelope, which depends only on x, does not rotate with the fringes. Hence, the ideal case for size measurements would be no displacement, where

$$I(x,y) \sim \cos 2\bar{k}\beta_o y \operatorname{sinc} 2\bar{k}bx \tag{45}$$

as shown in Figure 24(c).

Note that the square mentioned above was taken to be regularly oriented with respect to the instrument axes (Figure 24(a)); if it should be rotated to the position shown in Figure 24(d), the envelope becomes $\operatorname{sinc}^2(\bar{k}bx\sqrt{2})/2$. Hence, the position of the nulls from which measurements are made changes with object orientation and also with shape, as seen in the case of a circular object that has an envelope of the form

$$\frac{J_1(\bar{k}bx)}{\bar{k}bx} \quad .$$

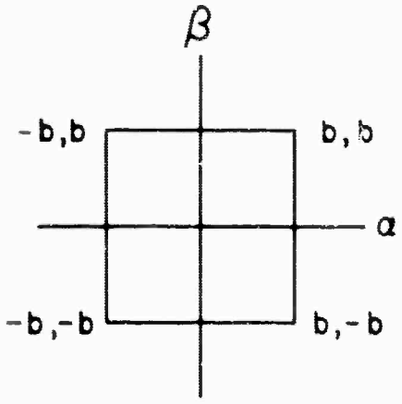

Figure 24(a). Square Object, Regularly Oriented

Figure 24(b). Fringe Patterns for Square Object (Figure 24(a)), Off-Axis

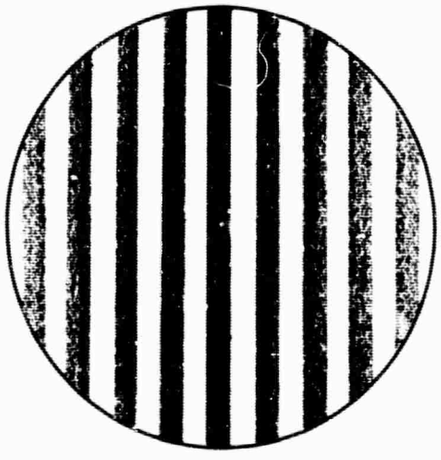

Figure 24(c). Fringe Patterns for Square Object (Figure 24(a)), On-Axis

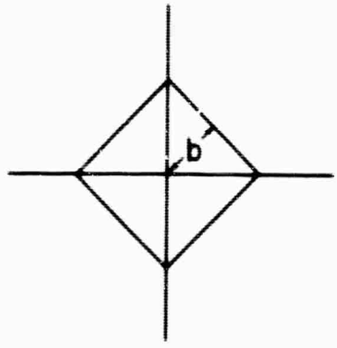

Figure 24(d). Showing Orientation of the Rotated Square

From the preceding discussion one may conclude that size measurements are possible for objects of known shape and orientation. Remaining is one important consideration that places the chief limitation upon the folding interferometer, i.e., introduction of a spectral bandwidth.

A single-point object angularly displaced some amount α along one axis with light of frequency bandwidth $2\Delta\nu$ has an intensity distribution given by

$$I(x, y, \Delta\nu) = \frac{1}{\Delta\nu} \int_{\bar{\nu} - \Delta\nu}^{\bar{\nu} + \Delta\nu} \left[1 + \cos 2k(\alpha x + \beta_o y) \right] d\nu \quad . \tag{46}$$

After integration, we obtain

$$I(x, y, \Delta\nu) = 2 \left[1 + \cos 2\bar{k}(\alpha x + \beta_o y) \operatorname{sinc} \bar{k} \left(\frac{2\Delta\nu}{\bar{\nu}} \right) (\alpha x + \beta_o y) \right] \quad . \tag{47}$$

To get usable cosine fringes, the frequency band envelope must not interfere within the aperture a; i.e., at worst, the principal maxima of the sinc would just fill the aperture. From this measurement, we may calculate a maximum angular displacement α_{max} that satisfies this condition for a given aperture size and frequency band,

$$\operatorname{sinc} \bar{k} \left(\frac{2\Delta\nu}{\bar{\nu}} \right) (\alpha_{max}\, a) = 1 \quad . \tag{48}$$

Hence,

$$\alpha_{max} = \frac{c}{4\Delta\nu a} \cdot \frac{\bar{\lambda}}{\bar{\lambda}} = \left(\frac{\bar{\nu}}{2\Delta\nu} \right) \frac{\bar{\lambda}}{2a} \quad ,$$

where $\bar{\lambda}/a$ is the beamwidth (BW). Providing there is shear in the system, there is no minimum angular displacement. In other words, the angular displacement α is confined to the range

$$0 \leq |\alpha| \leq \left(\frac{\bar{\nu}}{2\Delta\nu}\right) \frac{BW}{2} \tag{49}$$

Figures 25 through 28 demonstrate what would be seen in the aperture for values of $\bar{\nu}/2\Delta\nu$ equal to 2 (white light), 4, and 8, they also demonstrate the displacements of α equal to 1, 1-1/2, 2, and 3 beamwidths. As shown, for any chosen value of $\bar{\nu}/2\Delta\nu$, the ratio of frequencies of the sinc and cosine remain the same, and the angular displacement determines the number of maxima that will be viewed.

Calculations were also performed for a uniformly illuminated square of width 2b displaced an angular distance α_o. Integrating over the frequency bandwidth $\Delta\nu$, we have

$$I(x, y, \Delta\nu) = \frac{1}{2\Delta\nu} 8b^2 \int_{\bar{\nu} - \Delta\nu}^{\bar{\nu} + \Delta\nu} \left[1 + \cos \frac{4\pi}{c} \nu(\alpha_o x + \beta_o y) \operatorname{sinc} \frac{4\pi}{c} \nu bx\right] d\nu \quad . \tag{50}$$

This was done subject to the condition that sinc $(4\pi/c)\ \nu bx$ is slowly varying compared with cos $(4\pi/c)\ \nu(\alpha_o x + \beta_o y)$. We have then

$$I(x, y, \Delta\nu) = 8b^2 \left[1 + \frac{1}{2\Delta\nu} \operatorname{sinc} \frac{4\pi}{c} \nu bx \int_{\bar{\nu} - \Delta\nu}^{\bar{\nu} + \Delta\nu} \cos \frac{4\pi}{c} \nu(\alpha_o x + \beta_o y)\right] d\nu \tag{51}$$

and after integration over ν,

$$I(x, y, \Delta\nu) \simeq 8b^2 \left[1 + \operatorname{sinc} 2\bar{k}bx \cos 2\bar{k}(\alpha_o x + \beta_o y) \operatorname{sinc} \bar{k}\left(\frac{2\Delta\nu}{\bar{\nu}}\right)(\alpha_o x + \beta_o y)\right] \tag{52}$$

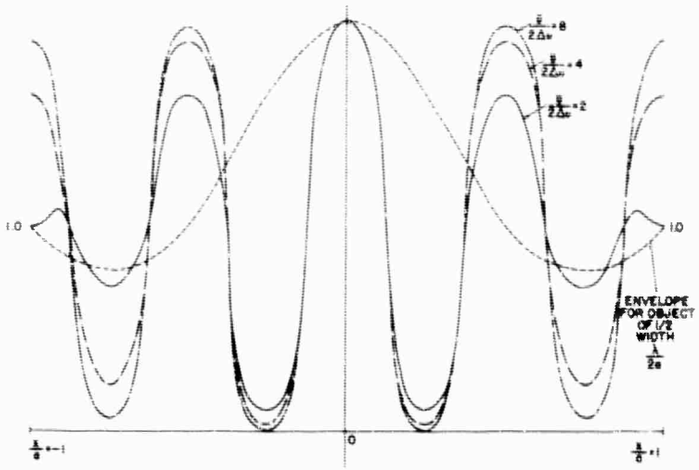

Figure 25. Point Object, $\alpha = \frac{\lambda}{a}$

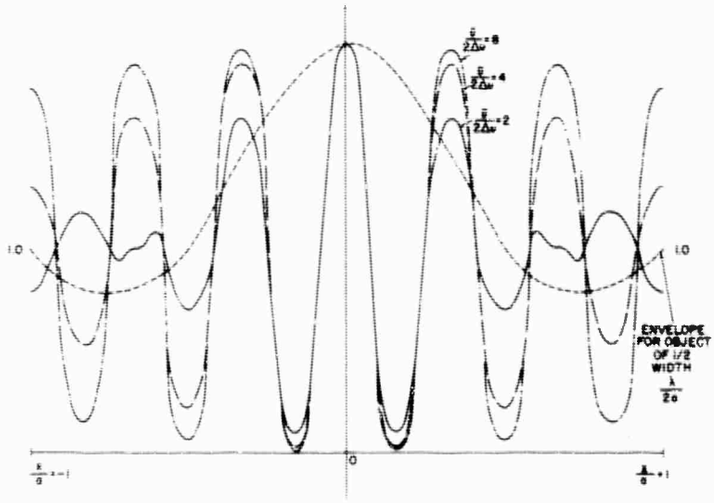

Figure 26. Point Object, $\alpha = \frac{3\lambda}{2a}$

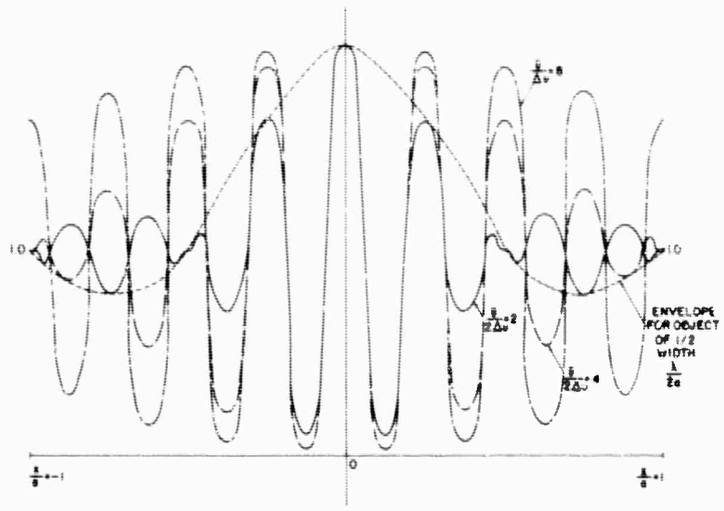

Figure 27. Point Object, $\alpha = \frac{2\lambda}{a}$

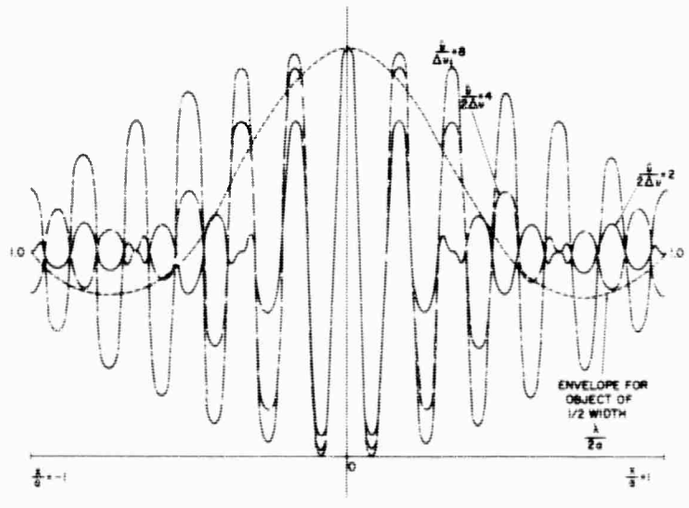

Figure 28. Point Object, $\alpha = \frac{3\lambda}{a}$

The condition mentioned above states essentially that the first zero ν_{os} of sinc $(4\pi/c)\,\nu bx$ must occur at a much larger value than the first zero ν_{oc} of cos $4\pi\nu/c\,(\alpha_o x + \beta_o y)$; that is

$$\nu_{os} >> \nu_{oc} \quad . \tag{53}$$

Since

$$\nu_{os} = \frac{c}{4bx} \quad \text{and} \quad \nu_{oc} = \frac{c}{8(\alpha_o x + \beta_o y)} \quad ,$$

this means that

$$2(\alpha_o x + \beta_o y) >> bx \quad . \tag{54}$$

When $\alpha_o = \beta_o$, we obtain

$$2\alpha_o(x + y) >> bx \tag{55}$$

or, at worst,

$$\alpha_o >> \frac{b}{2} \quad . \tag{56}$$

Equation (52) was solved on a computer for a few values of α_o and β_o. The results are presented in Figures 29 through 33. The purpose of showing the sequence is to illustrate the effect of nonstationarity of the interferometer. For $\Delta\nu/\bar{\nu} = 1/4$, the null required for determination of the square size becomes progressively fainter as α_o grows larger.

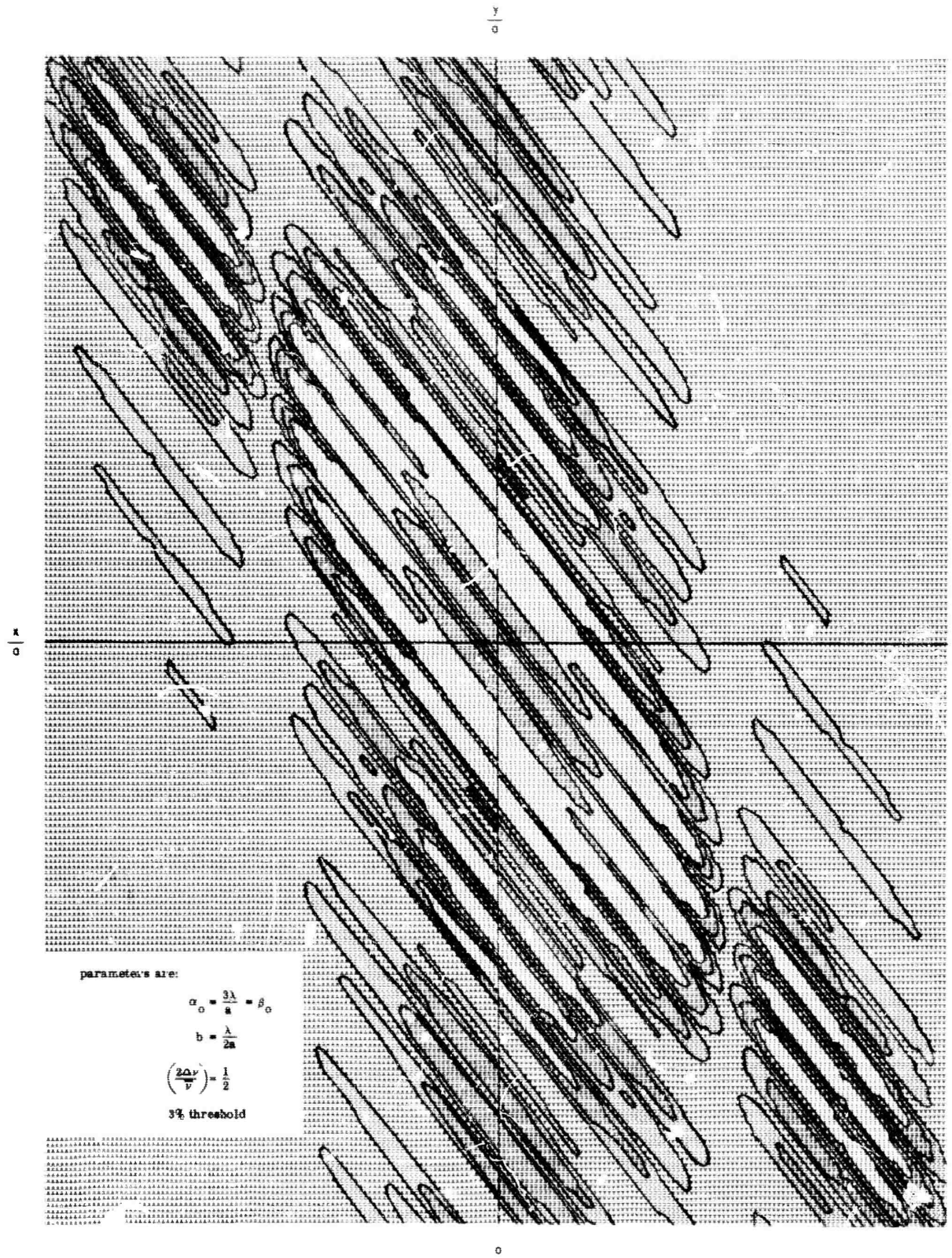

Figure 29. Showing Isophotes in the Fringe Pattern of a Square Object as Seen in the Folding Interferometer

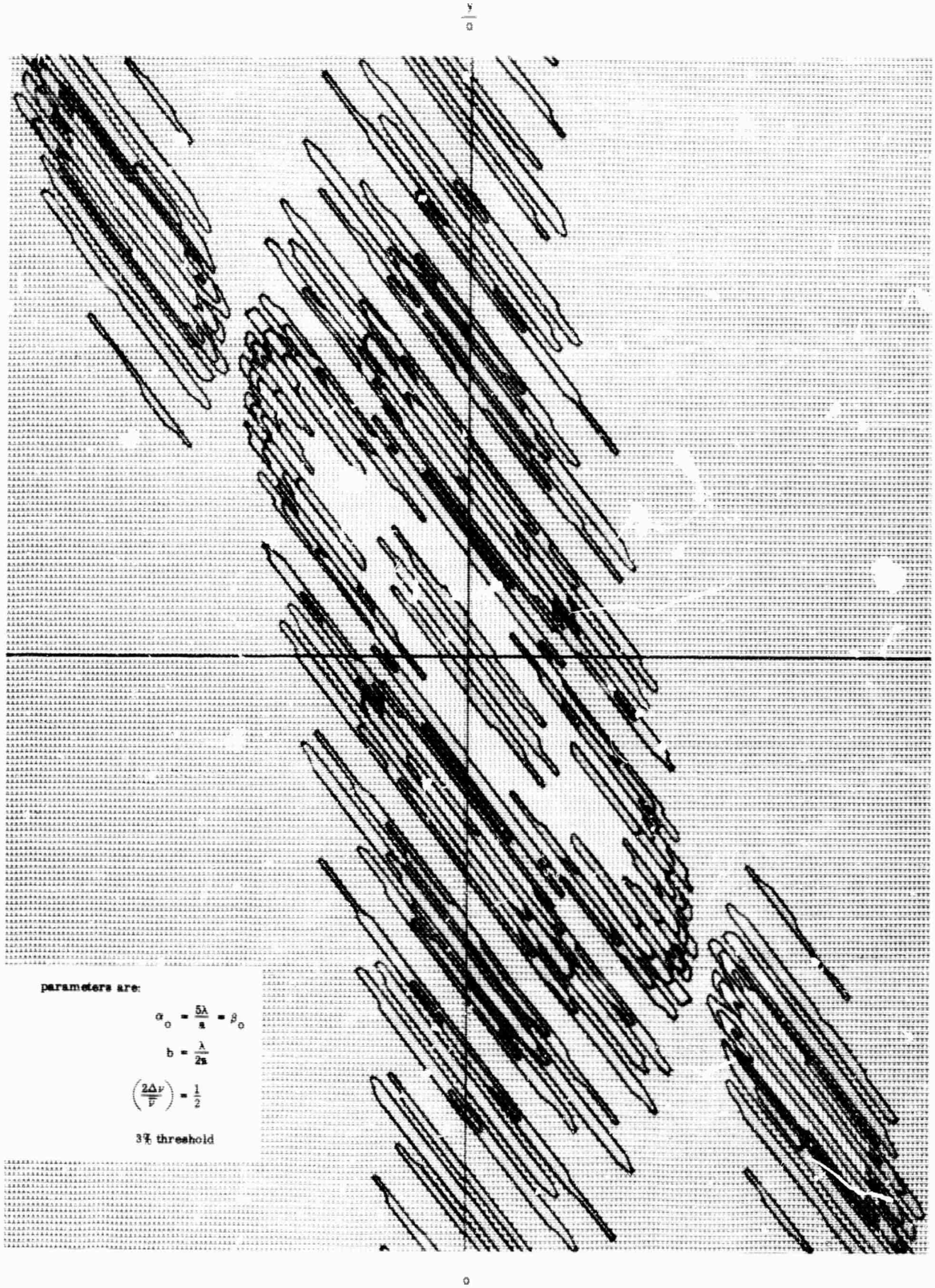

Figure 30. Showing Isophotes in the Fringe Pattern of a Square Object as Seen in the Folding Interferometer

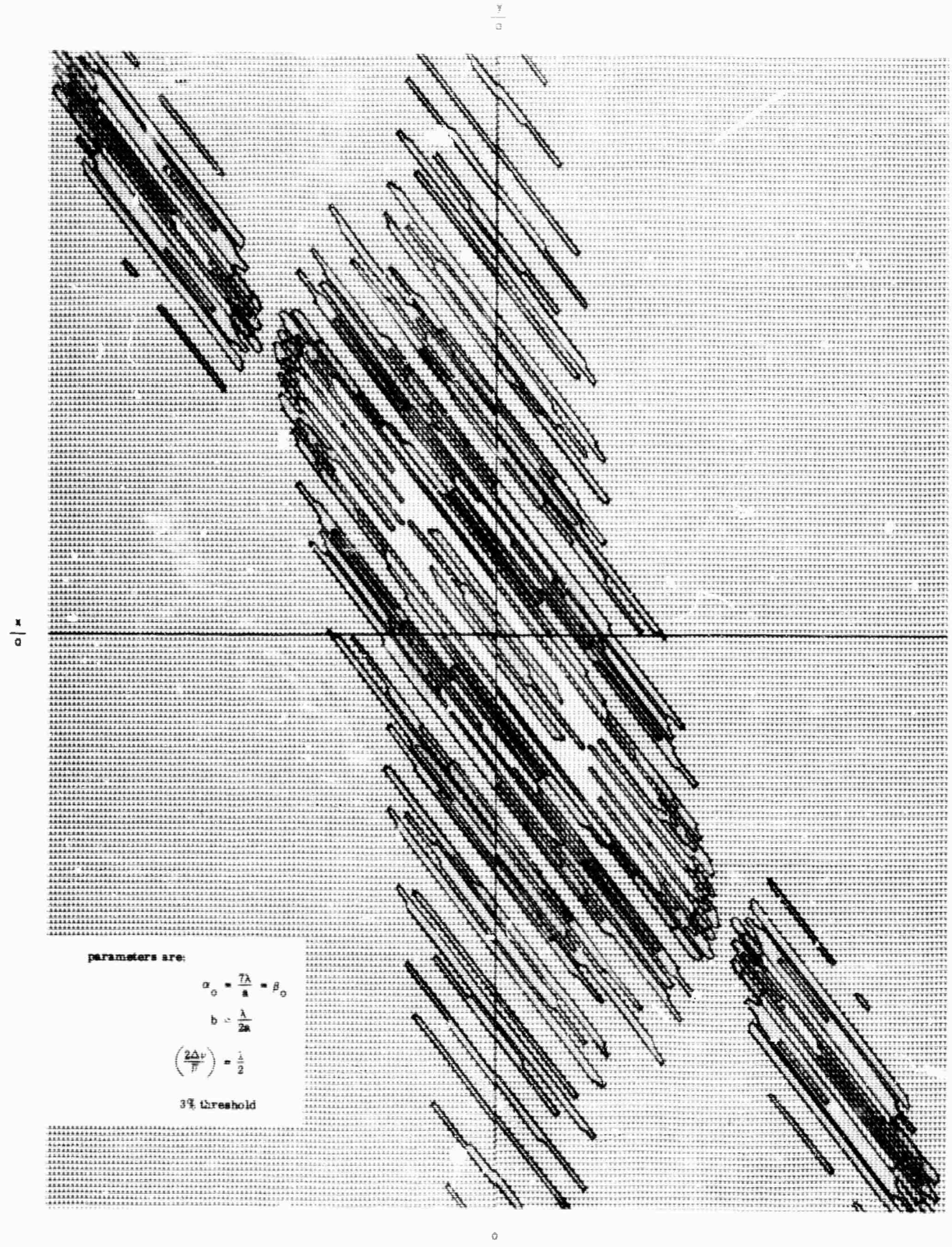

Figure 31. Showing Isophotes in the Fringe Pattern of a Square Object as Seen in the Folding Interferometer

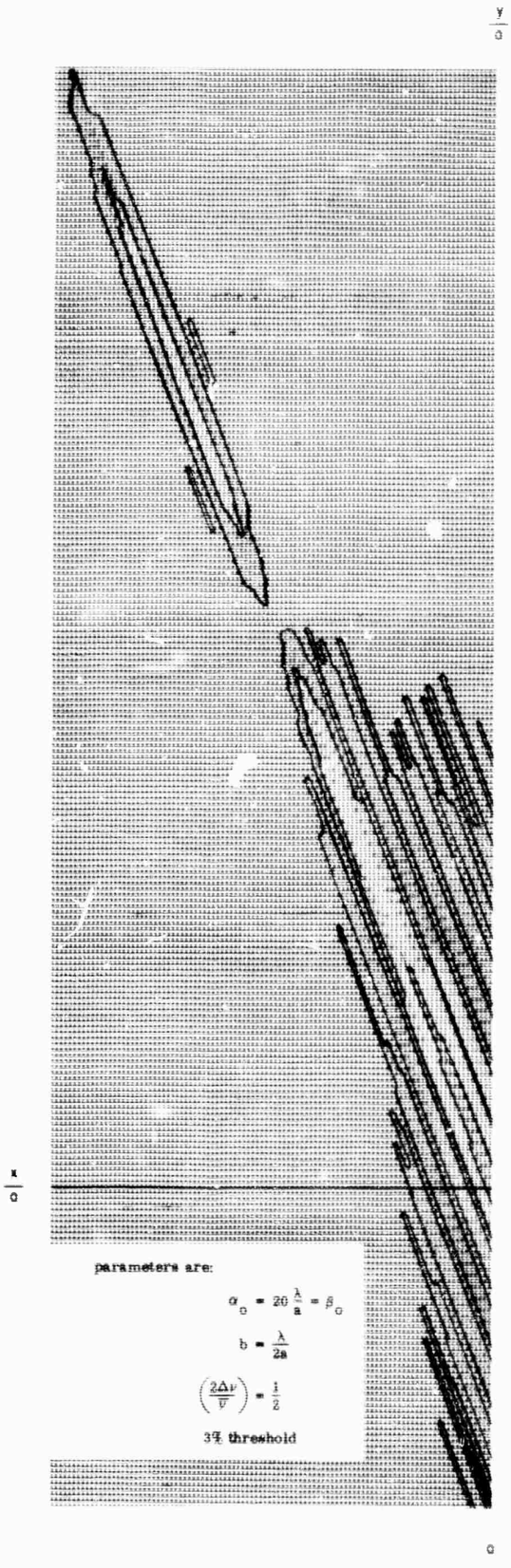

Figure 32. Showing Isophotes in the Fringe Pattern of a Square Object as Seen in the Folding Interferometer (because of space limitations only the left half of the figure is shown)

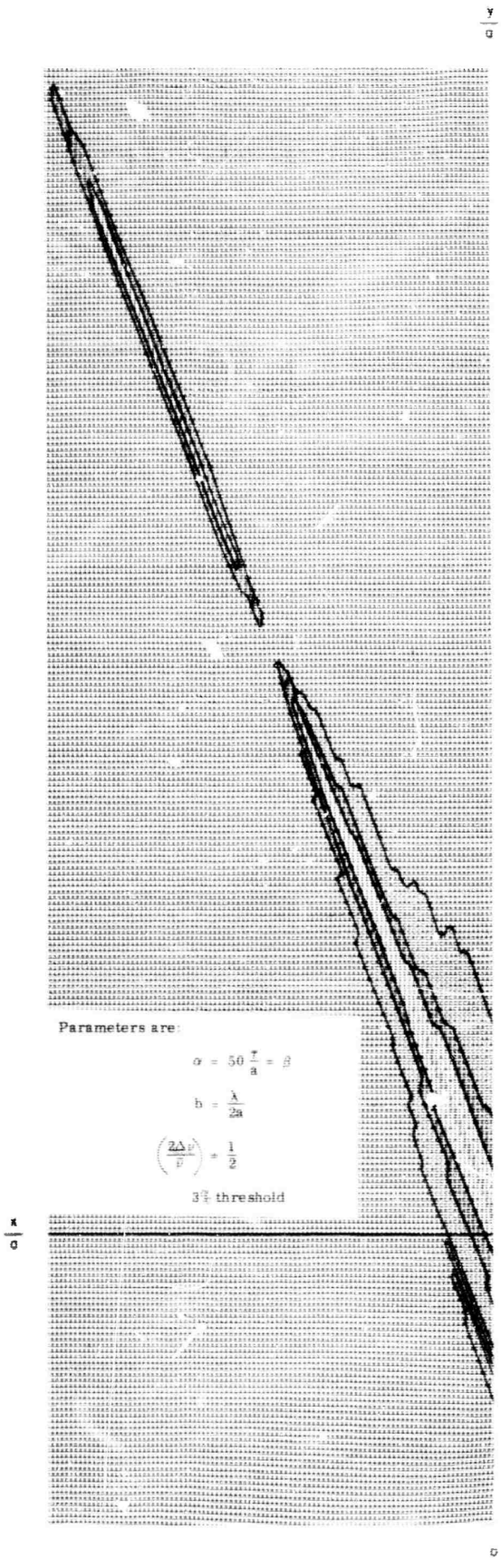

Figure 33. Showing Isophotes in the Fringe Pattern of a Square Object as Seen in the Folding Interferometer (because of space limitations only the left half of the figur. s shown)

MATHEMATICAL ANALYSIS OF THE FIZEAU INTERFEROMETER

We begin by calculating the impulse response for the Fizeau interferometer (see Figure 34).

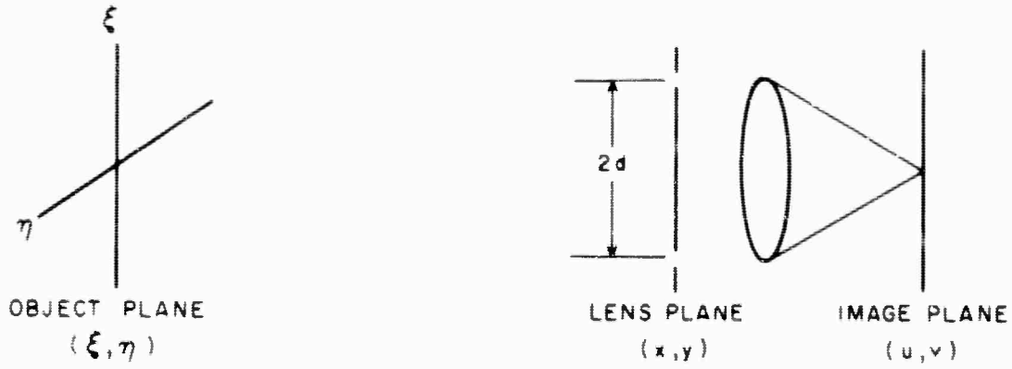

Figure 34. Relation of Object to Image Planes in the Fizeau Interferometer

If a point object is placed at ξ_o, η_o in the ξ, η plane, making angles α_o and β_o with respect to the ξ, η axes, the wave front striking the lens plane is tipped, and mathematically it may be represented by

$$e^{ik(\alpha_o x + \beta_o y)} \quad . \tag{57}$$

If we use the Green's function solution of the wave equation for this problem, the amplitude impulse response is given by the Fourier transform of this aperture amplitude distribution; i.e.,

$$A(u, v) = \int_{\text{aperture}} e^{ik(\alpha_o x + \beta_o y)} \, e^{\frac{-ik(ux + yv)}{f}} \, dx \, dy \tag{58}$$

If the pinholes in the lens plane are represented by δ functions, the aperture distribution is

$$\delta(x \pm d)\, \delta(y) = \delta(x + d)\, \delta(y) + \delta(x - d)\, \delta(y) \quad ,$$

and Eq. (58) becomes

$$A(u, 0) = 2 \cos kd\left(\alpha_o - \frac{u}{f}\right) .$$

The corresponding intensity impulse response is

$$\mathscr{I}(u, 0) = 4 \cos^2 kd\left(\alpha_o - \frac{u}{f}\right) , \tag{59}$$

and we immediately notice that the system is spatially stationary and independent of β_o.

Next we consider the intensity distribution for two-point objects, located at $\pm \alpha_o$ in object space. From Eq. (59) it is found to be

$$\mathscr{I}(u, 0) = c\left[\cos^2 kd\left(\alpha_o - \frac{u}{f}\right) + \cos^2 kd\left(\alpha_o + \frac{u}{f}\right)\right] , \tag{60}$$

where c is a constant. Equation (60) may be written as

$$\mathscr{I}(u, 0) = c\left[1 + \cos 2kd\, \alpha_o \cos 2kd\, \frac{u}{f}\right] . \tag{61}$$

If we consider $\cos 2kd\,\alpha_o$ as an envelope to determine resolution limits, then the minimum separation of the two points occurs when one cosine fringe is observable; i.e.,

$$\begin{aligned} 2kd\,\alpha_o &= \frac{\pi}{2} \\ 2\alpha_o &= \frac{\lambda}{4d} . \end{aligned} \tag{62}$$

Thus, $2\alpha_o$, the distance between the two points, must be about $\lambda/2d$ if we expect to resolve the two points.

Consider next a square resolvable source of uniform intensity distribution of angular size $2\Theta_o$, centered at the origin. If the object is incoherent and has an intensity distribution $f(\alpha\beta)$, its image intensity is given by the superposition integral

$$I(u, v) = \int_{-\infty}^{\infty} f(\alpha, \beta)\, \mathscr{L}(u, v \mid \alpha, \beta)\, d\alpha\, d\beta \quad , \tag{63}$$

where $\mathscr{L}(u, v \mid \alpha, \beta)$ is given by Eq. (59) for $v = 0$. Thus, for the square object mentioned above

$$I(u, 0) = \int_{-\Theta_o}^{\Theta_o} \int_{-\Theta}^{\Theta_o} 4 \cos^2 kd\left(\alpha - \frac{u}{f}\right) d\alpha\, d\beta \quad ,$$

and upon performing the integration, we obtain

$$I(u, 0) = c 2\Theta_o^2 \left[1 + \cos\left(2kd \frac{u}{f}\right) \operatorname{sinc} 2kd\Theta_o\right] \quad . \tag{64}$$

The visibility of these fringes is

$$V = \operatorname{sinc} 2kd\Theta_o \quad ,$$

and this function has its first zero when

$$2\Theta_o = \frac{\lambda}{2d} \quad . \tag{65}$$

The source size is determined from Eq. (65).

Consider the effects now of finite bandwidth. Suppose a quasi-monochromatic, incoherent point object having a frequency spread of $2\Delta\nu$ is angularly displaced an

amount α along one axis. The image intensity distribution may be obtained by superposition; i.e.,

$$I(u, \Delta\nu) = c \int f(\nu)\mathscr{L}(\alpha, u, \nu)\, d\nu$$

$$= \frac{c}{\Delta\nu} \int_{\bar{\nu} - \Delta\nu}^{\bar{\nu} + \Delta\nu} \left[1 + \cos 2kd\left(\alpha - \frac{u}{f}\right)\right] d\nu$$

$$= c\left[2 + \frac{1}{\Delta\nu} \int_{\bar{\nu} - \Delta\nu}^{\bar{\nu} + \Delta\nu} \cos\left[4\frac{\pi d}{c}\left(\alpha - \frac{u}{f}\right)\nu\right] d\nu\right] .$$

Upon integration and simplification, we obtain

$$I(u, \Delta\nu) = 2c\left\{1 + \cos 2\bar{k}d\left(\alpha - \frac{u}{f}\right) \operatorname{sinc}\left[2\bar{k}d\left(\alpha - \frac{u}{f}\right)\left(\frac{\Delta\nu}{\bar{\nu}}\right)\right]\right\} .$$

There is a fringe contrast due to the bandwidth, and this is given by the term

$$B = \operatorname{sinc} 2\bar{k}d\left(\alpha - \frac{u}{f}\right)\left(\frac{\Delta\nu}{\bar{\nu}}\right) .$$

The first zero of the contrast occurs when the argument of the sinc equals π. This implies that

$$u' \equiv \alpha - \frac{u}{f} \approx \frac{\bar{\nu}}{2\Delta\nu}\left(\frac{\bar{\lambda}}{2d}\right) . \tag{66}$$

From Eq. (66) we note that there is a limitation on the observation of the fringe pattern about the center of the pattern. Since the system is stationary, however,

there is no limitation on the off-axis angular distance α that may be tolerated; u' rather than u/f is the important variable.

The finite source calculation proceeds similarly. For incoherent sources it is permissible to weigh the quasi-monochromatic intensity with a frequency distribution and integrate over the frequency. Thus, using Eq. (64) with the source centered at α_o, we find

$$I(u, \alpha_o, \Delta\nu) = c2\Theta_o^2 \int f(\nu) \left[1 + \cos 2kd\left(\alpha_o - \frac{u}{f}\right) \operatorname{sinc} 2kd\,\Theta_o\right] d\nu$$

$$= \frac{c\Theta_o^2}{\Delta\nu} \int_{-\bar{\nu}-\Delta\nu}^{\bar{\nu}+\Delta\nu} \left[1 + \cos 2kd\left(\alpha_o - \frac{u}{f}\right) \operatorname{sinc} 2kd\,\Theta_o\right] d\nu \quad .$$

Assume that the sinc is slowly varying compared with the cosine. Then integration yields

$$I(u, \Delta\nu) = c\Theta_o^2 \left[1 + \operatorname{sinc} 2\bar{k}d\Theta \cos \frac{4\pi d\bar{\nu}}{c}\left(\alpha_o - \frac{u}{f}\right) \operatorname{sinc} \frac{4\pi d\Delta\nu}{c}\left(\alpha_o - \frac{u}{f}\right)\right] \quad . \quad (67)$$

Again the system is stationary and the finite frequency bandwidth restricts the instrument.

EXPERIMENTAL WORK

Since the stationarity of the Fizeau interferometer is so important, it was decided to check the point in a typical experiment. The experiment was only meant to be illustrative and was certainly not meant to be a detailed qualitative function of stationarity. In Figures 35, 36 and 37 microdensitometer traces are given for the interferometer fringe patterns resulting from measurement of a circular incoherent source placed alternately on-axis and off-axis. The geometry is given in Figure 38. The off-axis angular displacement was about 3^o, and the first zero in visibility occurred at about d = 1 cm. The finite spectral width of the line

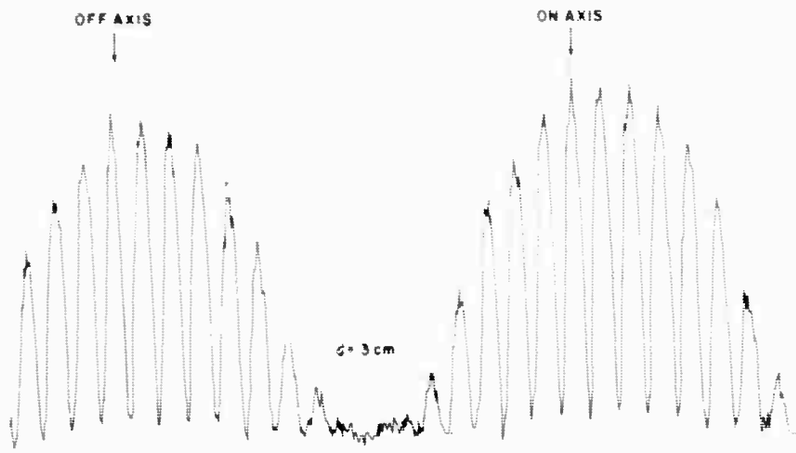

Figure 35. Microdensitometer Traces for the Fizeau Interferometer Image Patterns

(5461 Å/line, 80 Å spread) precluded measurement of the center point of more than about 0.6° for d = 0.3 cm. Figure 35 shows the fringe pattern for a separation of 0.3 cm; the fringes are high contrast and both off-axis and on-axis patterns are essentially the same. Figure 36 and 37 show the fringe pattern for separations of 0.5 cm and 1 cm. Again the patterns are much the same. The experiment then confirms the stationarity of the Fizeau interferometer for the conditions mentioned above.

SUMMARY

The conclusions drawn from this analysis and from the analysis presented in Chapter 2 are given in the next chapter. The instruments are compared primarily on their ability for measuring source sizes. Other advantages and disadvantages of the instruments are also included.

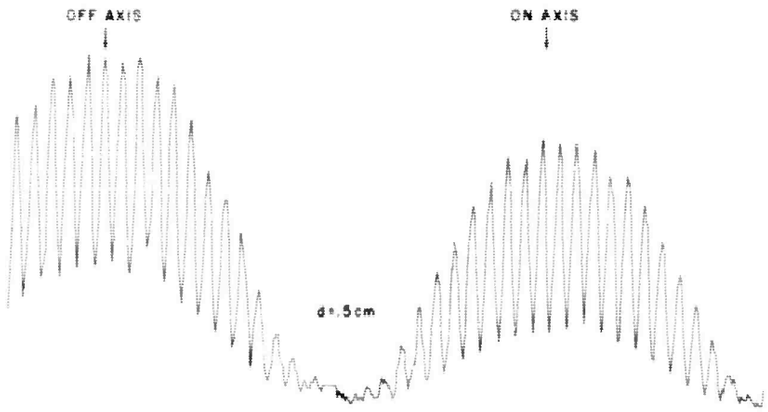

Figure 36. Microdensitometer Traces for the Fizeau Interferometer Image Patterns

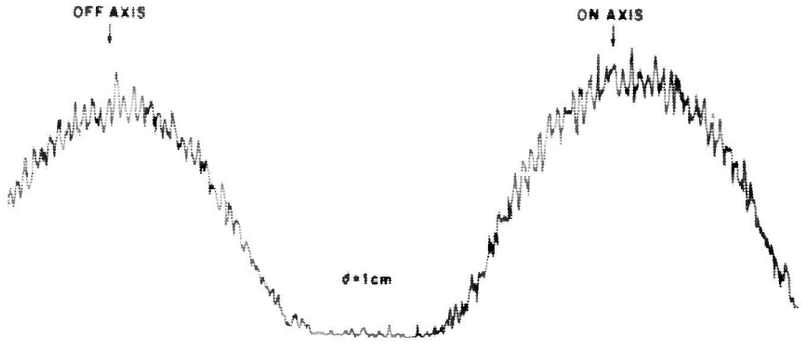

Figure 37. Microdensitometer Traces for the Fizeau Interferometer Image Patterns

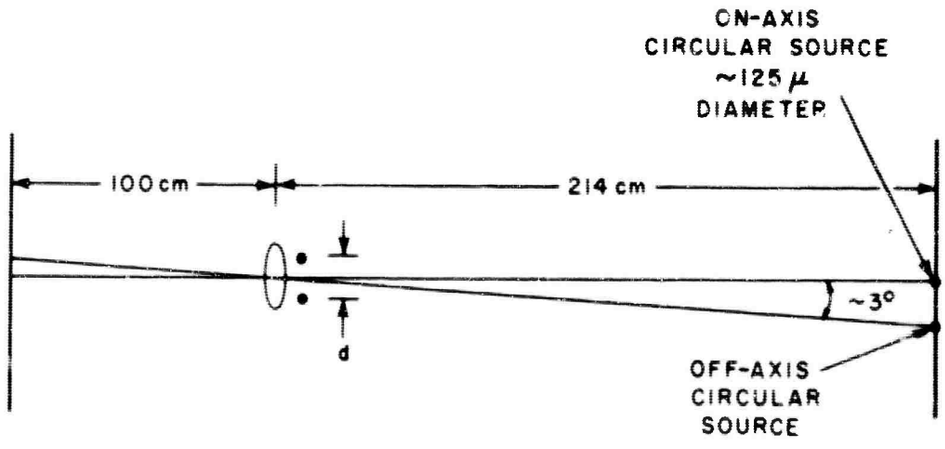

Figure 38. Experimental Geometry of the Fizeau Interferometer

CHAPTER 5

CONCLUSIONS

In this report we have considered interferometers and telescopes (reflecting and refracting) as instruments for measuring source sizes greater than a few microradians. We have also tried to point out limitations imposed upon both types of instruments by atmospheric conditions. In the absence of turbulence both instruments worked in the laboratory. The telescope is superior when observing resolvable objects because of its simplicity and because it enabled one to obtain a photographic record of the results with only one measurement. Even under these ideal conditions, the interferometers are, of course, sensitive to mechanical vibrations Visual detection of the fringes in the Michelson Stellar Interferometer was necessitated by the low light levels being used. In the presence of turbulence, however, it was soon clear that the interferometer was a superior instrument to the telescope for measuring source sizes of bodies having known configuration and intensity distribution.

Three different types of interferometers were investigated during the duration of this contract. A summary of the results of these investigations follows. From the analyses in Chapters 2 and 4 of the Fizeau, Michelson, and Folding interferometers, we shall compare their performance for measuring the angular size of known incoherent source shapes. The measurement of the internal distribution across unknown shapes will also be discussed.

COMPARISON OF THE FOLDING, MICHELSON, AND FIZEAU INTERFEROMETERS

MEASUREMENT OF ANGULAR DIAMETERS OF KNOWN SOURCES

All three interferometers may be used to determine the angular size of a known source configuration (e.g., a two point object or a uniformally illuminated square or disk), having a known intensity distribution. The limiting aperture size required for measurement of a square source is less by a factor of 3/4 in the folding interferometer than in the Fizeau interferometer.* For the two-point system, however,

* As seen in Table I we have defined the limiting aperture in the Fizeau interferometer as the slit separation whereas in the Michelson stellar interferometer the mirror separation is the limiting aperture and in the folding interferometer the mirror is the limiting aperture.

the minimum aperture sizes for all three interferometers must be the same, therefore, the factor of 3/4 mentioned above is not advantageous. The folding interferometer determines the size in a single measurement since a continuous aperture is used; in the Fizeau and Michelson interferometers a series of measurements are required. More knowledge about the possibility of constructing large folding interferometers is required before it is clear whether this single measurement feature is an advantage.

The chief disadvantage of the folding interferometer is the bandwidth limitation imposed by the nonstationarity of this interferometer. When the object is off-axis, the fringes may vanish unless $\Delta\nu/\bar{\nu}$ is made small enough. This effect is illustrated in Figures 29 through 33 where it is seen that the null in the fringe pattern becomes difficult to detect when a point object is more than a few bandwidths off-axis, or when the object has an angular diameter larger than a few bandwidths. It should be noted that these calculations were made for cases where the amount of shear in the instrument equals the angular size of the source. However, even if the shear remains constant, the fringes would disappear with increasing bandwidth. Also, their frequency increases as the object goes off-axis as seen from Eq. (52). The Fizeau interferometer is not sensitive to the position of the center of the object as was demonstrated experimentally for a typical case in Chapter 4. The lack of stationarity also makes the folding interferometer more sensitive to atmospheric turbulence than the Fizeau interferometer, since one effect of turbulence is often to change the apparent direction of the source. The nonstationarity of the Michelson interferometer also makes it more sensitive to atmospheric turbulence than the Fizeau instrument. If the object is non-resolvable, the calculations in Chapter 2 have shown that the nonstationarity in the Michelson interferometer does not affect the results in the absence of turbulence. In practice, this image motion due to turbulence forced us to use visual detection of the fringes. This problem, however, could be alleviated by electronic fringe detection.

Another disadvantage of the folding interferometer is that it measures a minimum rather than a null. The analytical calculations indicate that theoretically this is not very serious.

MEASUREMENT OF THE INTENSITY DISTRIBUTION OF UNKNOWN SOURCES

In principle, the Fizeau and Michelson interferometers may be used to measure the projected intensity distribution of any incoherent source. The coherence measurement yields the Fourier transform of source intensity, and it is only necessary to invert the transform. It is more difficult to do this experimentally for nonsymmetric sources, but in principle it can be done. It is not clear how this may be done in the case of the folding interferometer because, for two-dimensional objects, Eq. (39) does not permit the inversion to determine $I(\alpha, \beta)$. Perhaps some generalized folding procedure will permit this measurement, but a two-dimensional measurement is not possible given the present construction of the folding interferometer. Table 1 compares the important characteristics of the three interferometers and telescopes.

SUMMARY OF CONCLUSIONS

In summary we can say that in the absence of turbulence the telescope is the superior instrument for measuring bodies with angular diameters greater than a few microradians. It seems to be a fair conclusion that, if the source geometry and intensity distribution are completely unknown, then, source size determinations by interferometer techniques become impractical. When turbulence is present, it appears that an interferometer allows the best size measurement for sources of a known configuration.

TABLE I

COMPARISON OF FIZEAU, FOLDING, AND MICHELSON INTERFEROMETERS AND TELESCOPES

Parameter	Interferometer			Telescope
	Fizeau	Folding	Michelson	
Limiting Aperature (2d)	Slit separation	Full aperture	Mirror separation	Full aperature
Fringe Frequency	(1) Depends on slit separation (a) Insensitive to off-axis movement of source in x and y directions (b) Insensitive to off-axis movement of source in x and y directions, simultaneously	(1) Depends on folding angle of shear (a) Off-axis movement of source in x direction changes fringe frequency (b) Off-axis movement of source x and y directions does not change the fringes (c) Shear introduces fringes perpendicular to Fizeau fringes (d) Shear, x and y displacement cause a rotation	Constant depending on inner slit separation	No fringes
Stationarity	System is stationary	System is not stationary	System is not stationary	System is stationary
Two-Point Resolution	Points must be $\Theta = \lambda/4d$ apart if we expect to resolve them.	Points must be $\Theta = \lambda/4d$ apart if we expect to resolve them	Points must be $\lambda/4d$ apart if we expect to resolve them.	Diffraction limited
Source Size (S. S.) - Square	First zero of visibility curve gives a source size measurement $\Theta = S.S. = \frac{\lambda}{2d}$	First zero of visibility gives a source size measurement $S.S. = \Theta = \frac{3\lambda}{8d}$ A null not a zero needs a slightly smaller aperture.	First zero of visibility gives a source size measurement $\Theta = \frac{\lambda}{2d}$	Magnified image if square is resolvable by instrument
Source Size (S. S.) - Circular	$\Theta = 2.44\left(\frac{\lambda}{4d}\right)$	$\Theta = \frac{1.38\lambda}{2d} = \frac{2.76\lambda}{4d}$	$\Theta = 2.44\left(\frac{\lambda}{4d}\right)$	Magnified image if circle is resolvable by instrument
Bandwidth and Point Sources	Limits instrument. Spectral width sinc is in the same direction as fringes.	Limits instrument due to nonstationarity. Spectral width sinc along fringes causes them to wash out rapidly.	Limits instrument	No effect
Bandwidth and Finite Sources (a) Theoretical Limit (b) Practical Limit	(a) Bandwidth limits instrument (b) Limitation same	(a) Bandwidth limits instrument (b) Severe limitation in finding the null.	Bandwidth limits instrument severely for resolvable objects	No effect
Number of Measurement Required	Several	One	Several	One
Electrical Readout of Fringe Visibility	Feasible since fringe spacing constant	Very difficult	Feasible since fringe spacing constant	Not needed
Field of View	Same as Telescope	Determined by shear and object location	Better than telescope	~ d/focal length when viewing distant objects
Atmosphere	Moves fringes and diffraction pattern simultaneously	Fringes and diffraction pattern move at different rates due to nonstationarity	Same as for FOLDING	Smears image

REFERENCES

1. A.A. Michelson and F.G. Pease, Astrophys. J. 53, 249-259 (1921).

2. W.A. Calder, Bulletin of the Harvard College Observatory 885, 8-13 (1931).

3. J.L. Pawsey and R.N. Bracewell, "Radio Astronomy" (Oxford, England: The Clarendon Press, 1955).

4. R. Hanbury-Brown and R.Q. Twiss, Phil. Mag. 45 (7), 663 (1954).

5. B.J. Thompson and E. Wolf, J. Opt. Soc. Am. 47, 895 (1957).

6. B.J. Thompson, J. Opt. Soc. Am. 48, 95 (1958).

7. Block Associates, J. Opt. Soc. Am. 53 (2) (Feb. 1963) and 53 (5) (May 1963).

8. W.M. Sinton, Astron. J. 59, 369 (1954).

9. M.J. Beran, Optica Acta 5, 80 (1958).

10. G.B. Parrent and T.J. Skinner, Optica Acta 8, 93 (1961).

11. B.J. Thompson, J. Opt. Soc. Am. 54, 1406A (Nov. 1964).

12. R.A. Shore, Proceedings of Symposium on Electromagnetic Theory and Antennas, Copenhagen, Denmark, 787 (June 1962).

13. E.M. Linfoot and E. Wolf, Proc. Phys. Soc. London B69, 823 (1956).

14. C.A. Taylor and B.J. Thompson, J. Opt. Soc. Am. 48, 844 (Nov. 1958).

DOCUMENT CONTROL DATA - R&D

(Security classification of title, body of abstract and indexing annotation must be entered when the overall report is classified)

1. ORIGINATING ACTIVITY *(Corporate author)*

Technical Operations Research
Burlington, Massachusetts

2a. REPORT SECURITY CLASSIFICATION

Unclassified

2b. GROUP

3. REPORT TITLE

Relative Advantages of Interferometer Over Telescope for Measuring Source Sizes

4. DESCRIPTIVE NOTES *(Type of report and inclusive dates)*

Final Report Nov 63-Jan 65

5. AUTHOR(S) *(Last name, first name, initial)*

Hecksher, Helmut and Reynolds, George O.

6. REPORT DATE	7a. TOTAL NO. OF PAGES	7b. NO. OF REFS
March 65	82	17

8a. CONTRACT OR GRANT NO.	9a. ORIGINATOR'S REPORT NUMBER(S)
AF19(628)-3871	TO-B 65-19
b. PROJECT NO. 8663	
c. TASK 2	9b. OTHER REPORT NO(S) *(Any other numbers that may be assigned this report)* AFCRL-65-179
d.	

10. AVAILABILITY/LIMITATION NOTICES

Qualified requesters may obtain copies of this report from DDC

All other persons shall request through CFSTI

11. SUPPLEMENTARY NOTES	12. SPONSORING MILITARY ACTIVITY
Analysis of Michelson stellar, Fizeau double-slit, and the folding interferometers	Hq. AFCRL, OAR(CROI) United States Air Force Bedford, Massachusetts

13. ABSTRACT

In this report an analysis of the Michelson stellar, Fizeau double-slit and the folding interferometers is given and their relative merits are compared to a telescope for performing source size measurements. The atmospheric effects upon these instruments are examined. Experimental procedures describing the use of the Michelson stellar interferometer are given. Experimental difficulties encountered in the program are also discussed. It is concluded that interferometers are a better instrument than telescopes for source size measurements in the presence of a turbulent atmosphere if information about the source geometry and intensity distribution is available. When the source geometry and intensity distribution are not known, then none of the instruments give an absolute source size measurement under turbulent conditions. (Helmut Hecksher, and George O. Reynolds)

DD FORM 1 JAN 64 1473

14. KEY WORDS	LINK A		LINK B		LINK C	
	ROLE	WT	ROLE	WT	ROLE	
Interferometers Michelson Stellar Fizeau Double Slit Folding Atmospheric Effects on Interferometers Source Size Measurements Measurement of Angular Diameters Diffraction Physical Optica Telescopes						

INSTRUCTIONS

1. ORIGINATING ACTIVITY: Enter the name and address of the contractor, subcontractor, grantee, Department of Defense activity or other organization *(corporate author)* issuing the report.

2a. REPORT SECURITY CLASSIFICATION: Enter the overall security classification of the report. Indicate whether "Restricted Data" is included. Marking is to be in accordance with appropriate security regulations.

2b. GROUP: Automatic downgrading is specified in DoD Directive 5200.10 and Armed Forces Industrial Manual. Enter the group number. Also, when applicable, show that optional markings have been used for Group 3 and Group 4 as authorized.

3. REPORT TITLE: Enter the complete report title in all capital letters. Titles in all cases should be unclassified. If a meaningful title cannot be selected without classification, show title classification in all capitals in parenthesis immediately following the title.

4. DESCRIPTIVE NOTES: If appropriate, enter the type of report, e.g., interim, progress, summary, annual, or final. Give the inclusive dates when a specific reporting period is covered.

5. AUTHOR(S): Enter the name(s) of author(s) as shown on or in the report. Enter last name, first name, middle initial. If military, show rank and branch of service. The name of the principal author is an absolute minimum requirement.

6. REPORT DATE: Enter the date of the report as day, month, year, or month, year. If more than one date appears on the report, use date of publication.

7a. TOTAL NUMBER OF PAGES: The total page count should follow normal pagination procedures, i.e., enter the number of pages containing information.

7b. NUMBER OF REFERENCES: Enter the total number of references cited in the report.

8a. CONTRACT OR GRANT NUMBER: If appropriate, enter the applicable number of the contract or grant under which the report was written.

8b, 8c, & 8d. PROJECT NUMBER: Enter the appropriate military department identification, such as project number, subproject number, system numbers, task number, etc.

9a. ORIGINATOR'S REPORT NUMBER(S): Enter the official report number by which the document will be identified and controlled by the originating activity. This number must be unique to this report.

9b. OTHER REPORT NUMBER(S): If the report has been assigned any other report numbers *(either by the originator or by the sponsor)*, also enter this number(s).

10. AVAILABILITY/LIMITATION NOTICES: Enter any limitations on further dissemination of the report, other than those imposed by security classification, using standard statements such as:

(1) "Qualified requesters may obtain copies of this report from DDC."

(2) "Foreign announcement and dissemination of this report by DDC is not authorized."

(3) "U. S. Government agencies may obtain copies of this report directly from DDC. Other qualified DDC users shall request through _____."

(4) "U. S. military agencies may obtain copies of this report directly from DDC. Other qualified users shall request through _____."

(5) "All distribution of this report is controlled. Qualified DDC users shall request through _____."

If the report has been furnished to the Office of Technical Services, Department of Commerce, for sale to the public, indicate this fact and enter the price, if known.

11. SUPPLEMENTARY NOTES: Use for additional explanatory notes.

12. SPONSORING MILITARY ACTIVITY: Enter the name of the departmental project office or laboratory sponsoring *(paying for)* the research and development. Include address.

13. ABSTRACT: Enter an abstract giving a brief and factual summary of the document indicative of the report, even though it may also appear elsewhere in the body of the technical report. If additional space is required, a continuation sheet shall be attached.

It is highly desirable that the abstract of classified reports be unclassified. Each paragraph of the abstract shall end with an indication of the military security classification of the information in the paragraph, represented as *(TS), (S), (C), or (U)*.

There is no limitation on the length of the abstract. However, the suggested length is from 150 to 225 words.

14. KEY WORDS: Key words are technically meaningful terms or short phrases that characterize a report and may be used as index entries for cataloging the report. Key words must be selected so that no security classification is required. Identifiers, such as equipment model designation, trade name, military project code name, geographic location, may be used as key words but will be followed by an indication of technical context. The assignment of links, rules, and weights is optional.